AD NUMBER

AD812769

LIMITATION CHANGES

TO:

Approved for public release; distribution is unlimited.

FROM:

Distribution authorized to U.S. Gov't. agencies and their contractors; Critical Technology; 15 NOV 1966. Other requests shall be referred to U.S. Army Electronic Command, Attn: AMSEL-KL-TS, Fort Monmouth, NJ 07703. This document contains export-controlled technical data.

AUTHORITY

USAEC ltr, 30 Jul 1970

AD

HIGH VOLTAGE BREAKDOWN STUDY

Report No. 8

Eighth Quarterly Progress Report

16 August 1966 through 15 November 1966

Contract DA-28-043-AMC-00394(E)
AMC Task No. 7900.21.243.40.00
ARPA Order No. 517

Prepared for:

U.S. Army Electronics Command
Fort Monmouth, New Jersey

Prepared by:

Ion Physics Corporation
Burlington, Massachusetts

The work prepared under this contract was made possible by the support of the Advanced Research Projects Agency through the U. S. Army Electronics Command.

DISTRIBUTION STATEMENT

This document is subject to special export controls and each transmittal to foreign governments or foreign nationals may be made only with prior approval of CG, USAECOM, Attn: AMSEL-KL-TS, Fort Monmouth, New Jersey. 07703

ECOM

UNITED STATES ARMY ELECTRONICS COMMAND · FORT MONMOUTH, N.J.

NOTICES

Disclaimers

The findings in this report are not to be construed as an official Department of the Army position, unless so designated by other authorized documents.

The citation of trade names and names of manufacturers in this report is not to be construed as official Government indorsement or approval of commercial products or services referenced herein.

Disposition

Destroy this report when it is no longer needed. Do not return it to the originator.

HIGH VOLTAGE BREAKDOWN STUDY

Report No. 8

Eighth Quarterly Progress Report

16 August 1966 through 15 November 1966

Objective: To determine the factors influencing high voltage vacuum breakdown in conditions consistent with high power tube operation.

Contract DA-28-043-AMC-00394(E)

Technical Guidelines dated 27 March 1964

AMC Task No. 7900.21.243.40.00

ARPA Order No. 517

This report was prepared by:

M. J. Mulcahy and A. Watson

ION PHYSICS CORPORATION
Burlington, Massachusetts

[redacted]

TABLE OF CONTENTS

TABLE OF CONTENTS (Continued)

LIST OF ILLUSTRATIONS

PURPOSE

The factors influencing breakdown in high voltage vacuum devices will be studied. The information obtained will provide the basis for improvement in the design of microwave and modulator tubes that must operate at voltages greater than 100 kilovolts without breakdown.

ABSTRACT

The pilot experiment has been completed involving 32 treatments and 16 replications; of these, 23 involved full system bakeout. Procedures are used which yielded the significant unconditioned and conditioned data for electrode gaps ranging from 1.5 to 3.0 cm. The results have been statistically analyzed and a unified theory of breakdown has been developed which is consistent with the trends of this analysis. Finally, the 300 kv system has been maintained in a fully operational state and assembly of the magnetic field and energy storage systems has continued.

LECTURES, CONFERENCES AND PUBLICATIONS

Lectures and Conferences

1 September 1966

The monthly meeting to review progress on the contract was held at IPC. M. Chrepta from Fort Monmouth attended. The results to date and the program schedule to completion were discussed.

7-8 September 1966

The Second Symposium on Insulation of High Voltage in Vacuum was held at M. I. T. on 7-8 September 1966. A. S. Denholm, M. J. Mulcahy, J. Shannon, R. White and A. Watson attended from IPC.

14 September 1966

A Watson and M. J. Mulcahy visited P. Ingwersen of M. I. T., Lincoln Laboratory, for consultation on vacuum breakdown problems in the WL 8461 switch tube.

16 September 1966

A. Watson visited the Westinghouse Elmira plant to advise on vacuum breakdown problems in the WL 8461 switch tube.

20-22 September 1966

A. S. Denholm from IPC and G. W. Taylor from Fort Monmouth attended the 8th Conference on Tube Techniques sponsored by the IEEE Group on Electron Devices and held in New York.

12-14 October 1966

The 19th Gaseous Electronics Conference sponsored by the American Physical Society was held at Atlanta, Georgia on 12-14 October 1966. A. Watson from IPC attended.

28 October 1966

The monthly meeting to review progress on the contract was held at Fort Monmouth. M. J. Mulcahy and A. Watson from IPC, Professor H. Freeman from M. I. T., and M. Zinn, G. Taylor, M. Chrepta and J. Weinstein from Fort Monmouth attended. The statistical and physical analyses of the results of the pilot experiment were discussed and also the design of the initial experiment of phase II.

Publications

The following papers were presented during the reporting period.

"Prebreakdown Phenomena in Vacuum Gaps", A. Watson, A. S. Denholm, and M. J. Mulcahy, 2nd Symposium on IHVV, M. I. T. (1966) (see Appendix 4).

"Designed Experiments on High Voltage Vacuum Breakdown", M. J. Mulcahy, A. S. Denholm, A. Watson, G. W. Taylor, and M. M. Chrepta, 2nd Symposium on IHVV, M. I. T. (1966).

"Review of Highlights of the Second Symposium on Insulation of High Voltage in High Vacuum", A. S. Denholm, M. J. Mulcahy and G. W. Taylor, 8th Conference on Tube Techniques, New York (1966).

"Vacuum Breakdown as a Function of Gap Separation", A. Watson and M. J. Mulcahy, 19th Gaseous Electronics Conference, Atlanta, Georgia (1966).

1. INTRODUCTION

The work reported herein describes the eighth three months of a study of high voltage breakdown in vacuum with particular applications to problems encountered in the development of high power vacuum tubes.

The objectives of this period were as follows: maintain the 300 kv system in full operational state modifying and checking out where necessary; complete the pilot experiment and carry out a physical and statistical analysis of the results.

1.1 300 kv System

Eleven system and eight electrode bakeouts were carried out and thermocouple records indicate that satisfactory levels of temperature were attained. The high voltage bushing was assembled eleven times without problems and the backup ceramic column was delivered. The high voltage generator and monitoring apparatus have been maintained in an operational state and assembly of both the energy storage and magnetic field systems has continued.

1.2 Pilot Experiment

The pilot experiment has been completed: during this quarter the last 3 treatments in the 32 treatment experiment were carried out as well as 16 replicate treatments. For each treatment six gaps were examined in the range 0.5 to about 3.0 cm, yielding breakdown voltage and current data for unconditioned and conditioned electrodes at all gap spacings. The results have been analyzed both on a physical and statistical basis: theories of the breakdown mechanism have been developed and within the limits of the experimental error, the significance of the various important factors and two-factor interactions determined. Finally, the first experiment in Phase II has been designed.

2. 300 KV TEST VEHICLE

2.1 Vacuum Chamber

Eleven system and eight electrode bakeout cycles were completed during which no measureable chamber leaks developed. The mass spectrometer filament and likewise the valve seal on the roughing line were replaced during this period.

Prior to initiation of each test, the pressure in the chamber was low 10^{-7} to high 10^{-8} torr region for electrode only bakeout, and low 10^{-8} torr region for full system bakeout.

2.2 Baking System

Eleven full system bakeouts were successfully completed during the reporting period for a total of 20 for the pilot experiment alone. As reported in the previous Quarterly Progress Report the system was allowed to pump down for 24 hours before raising the temperature: this has eliminated the problem of severe outgassing above 200°C.

Again, the full baking cycle takes about 48 hours. The heaters are energized for 16 hours and this means that the electrodes are at about 400°C for 12 hours. After completion of system or electrode only bakeout the electrodes were allowed to cool to less than 50°C before voltage application. Thermocouple problems were enocuntered with the high voltage electrode and these have precipitated a redesign of the feedthrough connections on top of the bakeable column of the bushing.

2.3 High Voltage Power Supply

The high voltage power supply has operated satisfactorily and has provided precise voltage control and regulation up to 300 kv with an available current of greater than 200μA. The screens and the belt in the generator have been replaced as also has the oil in which is housed in high voltage cable termination. It seems desireable to carry out the latter operation after every 16 treatments.

2.4 Monitoring and Recording

The monitoring and recording apparatus has functioned satisfactorily providing records of the following parameters during each treatment:

- total X-radiation
- collimated X-radiation
- light output
- partial pressure
- gap current

2.5 Magnetic Field System

The magnet coils are complete and final checkout of the power supplies has been continued.

2.6 Energy Storage System

Assembly of the energy storage system is nearly completed and final design of the trigger circuit has been started. Stress relieving spinnings were delivered in the reporting period. This will enable preliminary testing of the unit to be carried out. It is hoped to check the system out initially using an air gap at atmospheric pressure.

2.7 Feedthrough Bushing

2.7.1 General

The feedthrough bushing was assembled eleven times during the reporting period. Only minor problems of contact between the springs and the rings were encountered. In some cases, one or two springs were broken, but it is of interest to note that this did not apparently effect the performance of the bushing. It seems also that the bakeable column has become more conditioned, evidenced by the reduction in magnitude or complete lack of pressure surges which were associated with gas release from the column.

2.7.2 Bakeable Column

The bakeable column has now undergone nineteen bakeouts which is in excess of most of the estimates of its lifetime in terms of heating cycles. The second ceramic column has been received from the General Electric Company.

2.7.3 Unbakeable Column

The glass-aluminum vinylseal bonded structure has operated satisfactorily during the reporting period.

2.8 Dielectric Envelopes

Quotations for the ceramic cylinders have been received and are being evaluated.

2.9 Electrodes

Nineteen sets of electrodes were tested and examined during this reporting period. Photomicrographs were taken of electrode surface damage and as previously described all breakdown markings were categorized.

3. THEORY OF BREAKDOWN MECHANISM

3.1 General

Refinements have been made to the analysis of a model dc breakdown mechanism for long vacuum gaps. The analysis is not complete but enough has been developed to present a qualitative picture of what is happening. In particular, it can explain experimentally observed behavior of the prebreakdown current as a function of voltage and gap separation. It is also capable of describing the conditions of instability for which the prebreakdown current will run away to complete gap failure.

The model describes the accumulation of gas in the interelectrode space after evolution from the anode due to electron beam heating. Consequently the pumping conductance of the electrode geometry is expected to be a significant factor. This is apparently borne out by the results of the partial factorial experiment.

3.2 Cathode Emitting Conditions

The field strength at the surface of a cathode protrusion is compounded from two sources. A purely geometrically enhanced field, βE, is always present but this is supplemented by an ionic space charge field generated as an ion current flows to it from the interelectrode space. The ionization arises from interaction of the field emitted electron beam with gas evolved from an anode hot spot by diffusion from inside the metal. Thus the magnitude of this ionization depends critically upon the capability of the anode to deliver gas to the surface. It is believed that this condition of the anode specifies in physical terms the "degree of conditioning" which at the present is a parameter which is only arbitrarily defined.

The total field strength, E_S, is:

$$E_S = \beta E + X_S = \frac{\beta V}{d} + X_S \qquad (1)$$

where:

V = applied voltage
d = gap separation
β = field enhancement factor

Application of voltage to the emitting tip results in surface atom migration and the establishment of a local radius of curvature, r, and

$$\beta E = \frac{BV}{d} = \frac{V}{kr} \tag{2}$$

There is thus a relationship between the enhancement factor and gap separation. The equilibrium radius of curvature is related to the surface field strength E_S; thus:

$$rE_S^2 = 12\pi\gamma \tag{3}$$

where γ = surface tension of cathode material. Hence, from Equations (1), (2) and (3):

$$\frac{1}{E_S} = \frac{V}{12\pi\gamma k} + \frac{X_S}{E_S^2} \tag{4}$$

The area of the surface of the tip from which most electrons are emitted can be defined by a cone angle ψ from the axis. It is:

$$2\pi(1-\cos\psi)\,r^2$$

and therefore it is dependent on the local field, E_S. Therefore:

$$\text{Area} = 2\pi(1-\cos\psi)r^2 = 2\pi(1-\cos\psi)\left(\frac{12\pi\gamma}{E_S^2}\right)^2$$

The total current, I_F, emitted by the Fowler-Nordheim effect is thus:

$$I_F = AE_S^2 \exp\left(-\frac{B}{E_S}\right) \cdot 2\pi(1-\cos\psi)\left(\frac{12\pi\gamma}{E_S^2}\right)^2$$

Therefore:

$$I_F = \alpha E_S^{-2} \exp -\left(\frac{B}{E_S}\right) \tag{5}$$

where

$$\alpha = \left[144\pi^3\gamma^2 2(1-\cos\psi)\right]$$

It is noteworthy that this equation predicts a current maximum as E_S increases. If this were the total electron current, then no runaway would be possible from a single protrusion. It is however supplemented by the flow I_i of electrons generated in the interelectrode space by ionization of the gas there. Thus:

$$I = I_F + I_i \tag{6}$$

A section of the beam of depth dz situated at a distance z from the cathode will contribute an increment of electron density $d\dot{N}_e$ generated per second due to ionization of the intercepted gas which may be present.

$$d\dot{N}_e = N\sigma_i I\, dz \tag{7}$$

where σ_i = cross section for ionization.

Assuming that all the electrons so created are collected by the anode, the supplementary electron current, I_i, can be calculated:

$$I_i = \int N\sigma_i I\, dz \tag{8}$$

In Appendix 1 it is shown that: if the gas density is low then

$$\left| I_i \right| = \left| I_+ \right| \text{ and } I \approx I_F \tag{9}$$

This approximation will be assumed in the following text to describe prebreakdown current phenomena.

Up to this point no account has been given of the rate of growth of gas density between the electrodes or of its contribution in defining the level of ionic space charge enhancement X_S. For this, it will first be necessary to study the conditions at the anode and derive an expression for the rate of gas evolution. The pumping conductance of the gap will then control the gas density in the electron beam and hence the ionization.

3.3 The Anode Conditions

An electron beam spreading from a cathode protrusion has a radius R at the anode. The power delivered, IV, over the resultant hot spot will raise the temperature T above the ambient value T_a according to the conditions for thermal conductive equilibrium there. Thus:

$$T - T_a = \frac{W}{4KR} \tag{10}$$

This elevated temperature raises the value of the diffusion coefficient D of hydrogen gas inside the metal:

$$D = D_o \exp \left\{ -\frac{H}{kT} \right\} \tag{11}$$

where H = activation energy for diffusion.

The rate of evolution of gas per square cm of surface per second can be derived by consideration of gaseous diffusion to a hot spot on the anode surface (Appendix 2). The approximate result is:

$$\dot{N} = 4RD_o n \exp \left\{ -\frac{H}{kT_m} \right\} \tag{12}$$

Where n = gas density deep inside the anode and T_m is a weighted mean value of temperature at the surface and the ambient value.

Taking:

$$T_m \cong 1/2 \, (T_S + T_a) \tag{13}$$

then:

$$T_m = T_a + 1/2 \, (T_S - T_a) = T_a + \frac{IV}{8 K R}$$

and Equation (12) becomes:

$$\dot{N} = 4 R D_o n \exp \left\{ -\frac{H}{k \left(T_a + \frac{IV}{8KR} \right)} \right\}$$

It is convenient to represent the hot spot radius R in terms of the gap separation d. Hence from Chatterton's formula[1] and Equation (2):

$$R = 2d^{1/2} (\beta r)^{1/2} \sin \psi = \lambda d \tag{15}$$

where:

$$\lambda = 2k^{1/2} \sin \psi \tag{16}$$

Hence:

$$\dot{N} = 4D_o \lambda n d \exp \left[-\frac{H}{k \left(T_a + \frac{IV}{8K\lambda d} \right)} \right]$$

$$= g d \exp \left[- \frac{H}{k \left(T_a + \frac{IV}{8 K \lambda d} \right)} \right] \tag{17}$$

where:

$$g \equiv 4 D_o \lambda n \tag{18}$$

is a function of the gas density n deep inside the anode and also of the parameter D_o which is characteristic of the anode material. This "gas supply parameter" controls the ionization in the gap and through it both the total electron current and the space charge field enhancement.

Now putting:

$$\left. \begin{aligned} \frac{H}{k} &\equiv \Theta \\ 8 K \lambda &\equiv f \end{aligned} \right\} \tag{19}$$

then:

$$\dot{N} = gd \exp \left[- \frac{\Theta}{T_a + \frac{IV}{fd}} \right] \tag{20}$$

3.4 The Gap Conditions

The expression for the equilibrium gas density on the gap axis can be estimated by defining a pumping conductance S for the gap:

$$S = \frac{\dot{N}}{\Delta N} \tag{21}$$

where $\Delta N \cong N$ is the differential of molecular number density between the gap axis and its periphery. Hence:

$$N = \frac{\dot{N}}{S} \tag{22}$$

An analysis of S as a function of gap separation is given in Appendix 3. Assuming that equal numbers of electrons and singly ionized atoms are generated by impact within the volume of the primary electron beam, the ion current drifting to the cathode can be calculated if all these are assumed to be collected at the electrodes. Hence, from Appendix 1.

$$\left|I_+\right| = \left|I_i\right| = I_F \frac{N\sigma_o d}{V} \ln\left(\frac{V}{U_i}\right) \tag{23}$$

and the total electron current I_e is:

$$I_e = I_F + I_i = I_F \left\{1 + \frac{N\sigma_o d}{V} \ln\left(\frac{V}{U_i}\right)\right\} \tag{24}$$

It is important to outline the assumptions made in deriving this result. They are:

(1) There is no ionization loss by recombination.
(2) Ions and electrons proceed directly along the beam without diffusion from it.
(3) Only single ionization events are accounted for.

Whilst these are undoubtedly approximations, an exact analysis would contribute so much complexity as to obscure the main physical reasoning.

The contribution of the ion current to the enhancement of the field strength at the emitting tip may now be calculated.

3.5 Positive Space Charge Field at the Emitter Tip

Low density gas when present between the electrodes will intercept the primary electron beam injected from the cathode by field emission. The resultant ions and electrons will accelerate freely with few collisions and give rise to additional ion and electron currents. If enough positive ions are present at any point the electric field strength will be increased on the cathode side and reduced on the anode side. The additional field at the cathode surface can be calculated by integrating Poisson's equation (Appendix 1). The result is:

$$X_S^2 = \frac{J_F \sqrt{V}}{\sqrt{\frac{2e}{m_e}}} \left[\frac{2N\sigma_o(\mu - 1)d}{3V\sqrt{V}\sqrt{U_i}} - 1\right] \tag{25}$$

and since $N = \dot{N}/S$ and:

$$J_F = \frac{I_F}{2\pi(1 - \cos\psi)r^2} = \frac{I_F E_S^4}{2(12\pi\gamma)^2(1 - \cos\psi)} = \frac{I_F E_S^4}{\alpha} \tag{26}$$

then:

$$\frac{X_S^2}{E_S^4} = \frac{I_F \sqrt{V}}{\alpha \sqrt{\frac{2e}{m_e}}} \left[\frac{2\dot{N} \sigma_o (\mu - 1) d}{3 S V \sqrt{V U_i}} - 1 \right] \tag{27}$$

Substituting for $\dot{N}$ from Equation (20):

$$\left(\frac{X_S}{E_S^2} \right)^2 = \frac{I_F \sqrt{V}}{\alpha \sqrt{\frac{2e}{m_e}}} \left[\frac{2 \sigma_o (\mu - 1)}{3V \sqrt{V U_i}} \left(\frac{g d^2}{S} \right) \exp \left\{ - \frac{\Theta}{T_a + \frac{IV}{fd}} \right\} - 1 \right] \tag{28}$$

The term gd^2/S is dependent only on the density of dissolved gas in the anode, the basic diffusion coefficient D_o for the material and the electrode geometry. These factors then play a major role in determining the ionization field enhancement at the cathode.

It remains now to find a value of I_F which will satisfy the above equation simultaneously with Equation (5).

3.6 Current as a Function of Voltage

In the preceeding analysis expressions have been derived for the field emission current I_F as a function of E_S, the total surface field strength at the cathode projection. The total surface field strength is a combination of contributions from the geometrical field enhancement due to the shape of the tip and from the space charge field X_S of the surrounding ions.

In a separate analysis an arbitrary current strength I_F has been assumed and from this has been derived the ionic space charge field X_S, which in turn controls I_F. Voltage has been an implicit parameter in these derivations and it now remains to develop a means of solving the expressions simultaneously by eliminating X_S and in such a way as to explain the experimentally demonstrated behavior of current and voltage at different gap separations. A graphical method of solution can be devised as follows:

The field emission current is a function of $1/E_S$ which, from Equation (4), is expressed as $V/12\pi\gamma k + X_S/E_S^2$. A new variable is now defined:

$$y = \frac{1}{E_S} - \frac{V}{12\pi\gamma k} = \frac{X_S}{E_S^2} \tag{29}$$

The field emission current can be plotted in terms of y by a simple shift of the origin by the amount $V/12\pi\gamma k$ (see Figure 1).

Now constructing a graph with y and I_F as the ordinate and abscissa axes, the Equation (28) for X_S/E_S^2 can be plotted directly on this for fixed values of voltage and gap separation. A graph of I_F as a function of y can be superimposed on the same diagram using the shift of origin which has just been described (see Figure 2).

The asymptotic form of y (I_F) is:

$$y \rightarrow \text{const}\sqrt{I_F}$$

where the constant increases with the gas supply parameter g and is inversely proportional to the square root of the voltage. The gas supply parameter g thus fixes the scale of the asymptotic parabola I_F in Figures 2 and 3 which show two possible configurations. There may thus be one or three solutions for I_F.

The stability of any solution is the criterion for breakdown but this will not be dealt with yet because the approximation $I \cong I_F$ is being assumed and the runaway cannot be adequately described without modifications to the present simple procedure. A perturbation analysis must be made to derive the condition for current instability which is the breakdown condition. Before proceeding to a perturbation analysis it can be inferred from the experimental evidence that the value of y must be small.

If y is small then Equation (29) reduces to the form:

$$VE_s = 12\pi\gamma k$$

and since:

$$E_s \approx \frac{\beta V}{d}$$

then:

$$V^2 \propto d$$

which is observed experimentally for fully conditioned electrodes. Deviation from this ideal law however for inconditioned electrodes suggests that breakdown takes place at significantly large values of y.

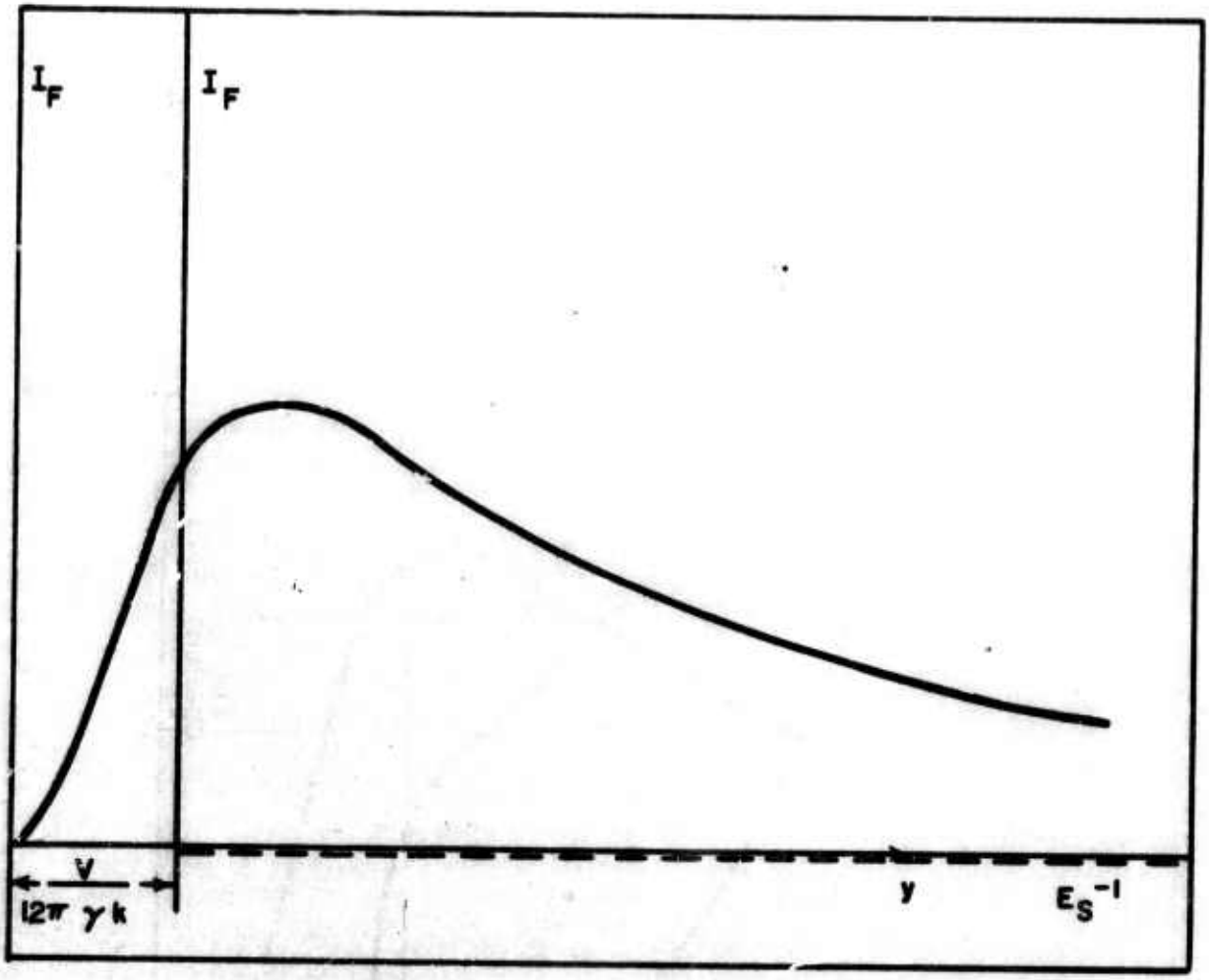

Figure 1. I_F as a Function of y and $\frac{1}{E_s}$

-1929

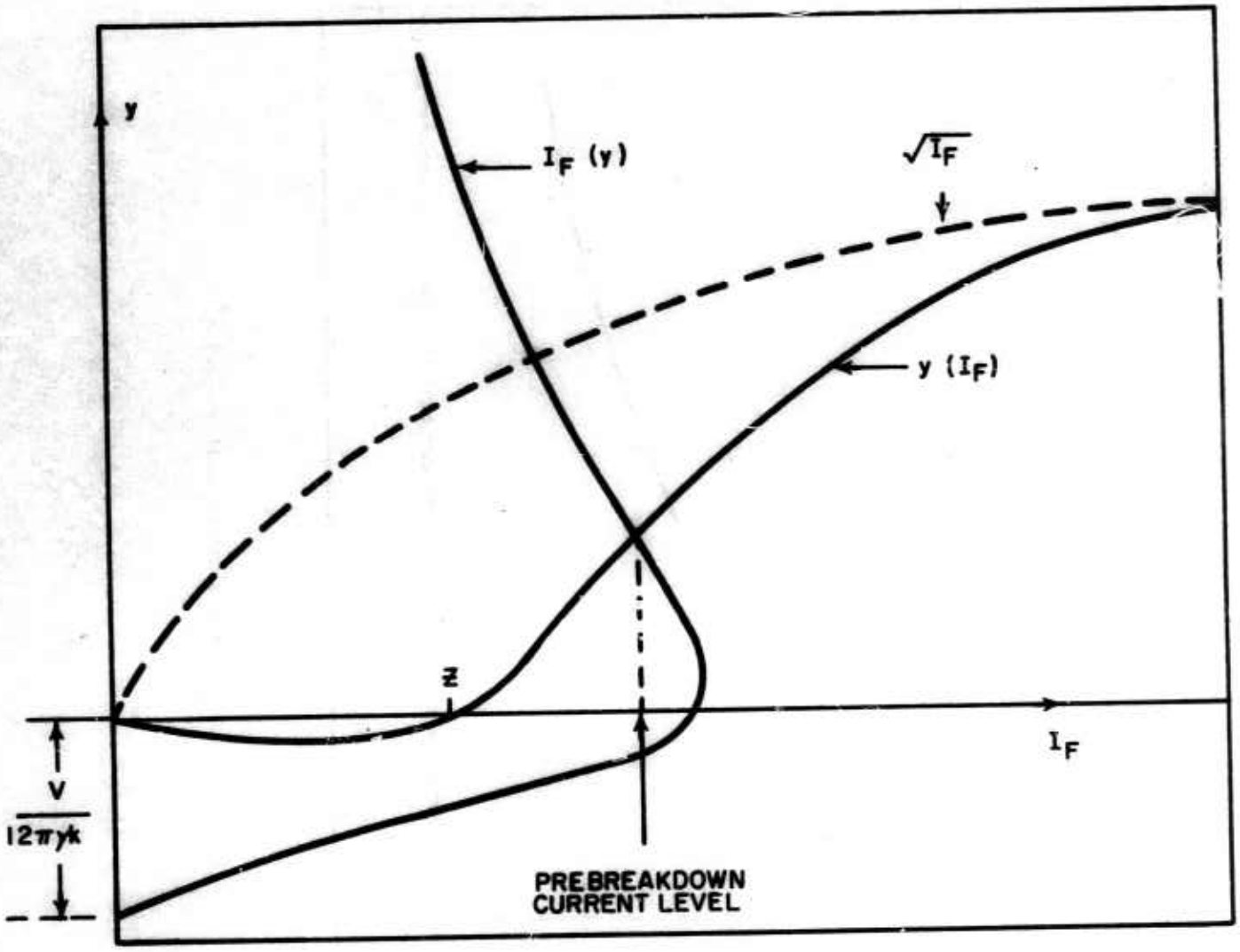

Figure 2. Graphical Method For Determining Prebreakdown Currents

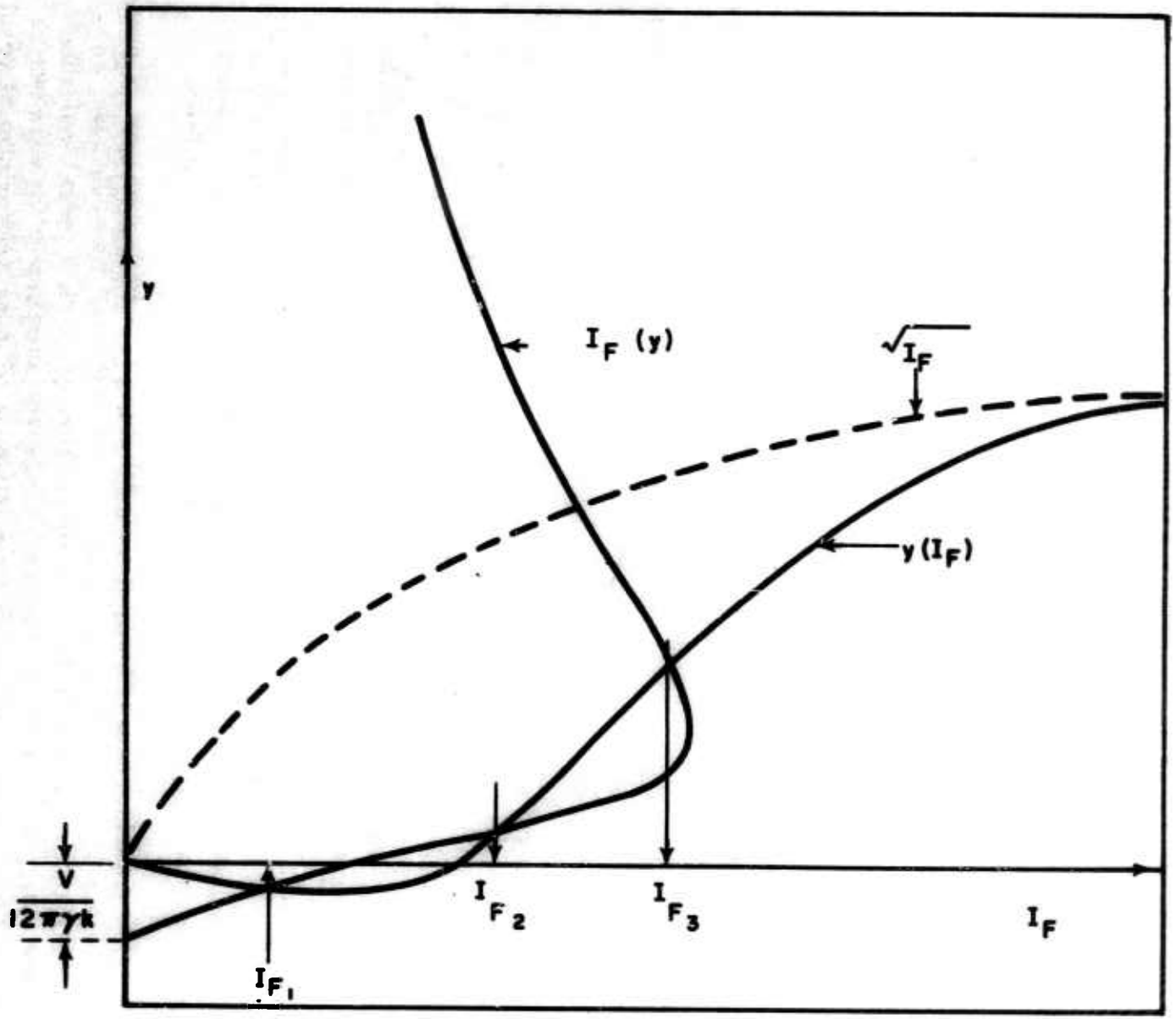

Figure 3. Alternative Condition to Figure 2 Showing Multiple Solutions

Hence the unstable point lies close to the I_F axis in the diagrams unless deviations from linearity on the plot of V_B vs $d^{1/2}$ occur.

3.7 Properties of the Solutions

Figure 4 shows how a solution of Equations (5) and (28) may be obtained. The behavior, however, of the current as voltage increases can only be obtained by studying the position of the intersection points for two networks of curves, each pair representing a different voltage.

A set of curves is sketched in Figure 4. The point Z(y = o) can be seen by some manipulation of Equation (28) to move with increasing voltage firstly towards the origin and then back again. In consequence of this the corresponding current solution will also fall at first and then rise as voltage increases. This has been observed experimentally and is shown in Figure 5.

The physical reason for this is that there are two competing processes determining the total ionization space charge. The gas evolution rate increases with applied voltage and the cross section for ionization decreases[2].

At low voltage the cross section variation dominates but eventually there is a reversal as the gas evolution rate rises. Thus the field emission current falls to a minimum and then rises.

Many unusual properties of prebreakdown current behavior can be explained in terms of this. It is characterized by the position of the point Z in Figure 2. At this point y is zero and there is no resultant space charge field enhancement. When the gas evolution rate is rising with voltage faster than the rate of reduction of ionization cross section, Z moves to the right to higher values of I_F. When gas evolution rate is rising with voltage at a lower rate than the reduction of ionization cross section then it moves to the left. The result is to cause either a rise or fall of I_F with voltage.

A corollary to this is that at any point Z there are two possible $y(I_F)$ curves passing through it corresponding to different voltages. For one intersection with $I_F(y)$ the current rises with V and for the other it falls.

Consider now the way in which y changes with gap separation d for any one value of V. The point Z always moves to the left towards lower currents. Similarly there will be two y curves through each Z point, indicating different voltages. A dual breakdown voltage with corresponding currents is shown in Figure 6 which provides some evidence of this. (experimental result).

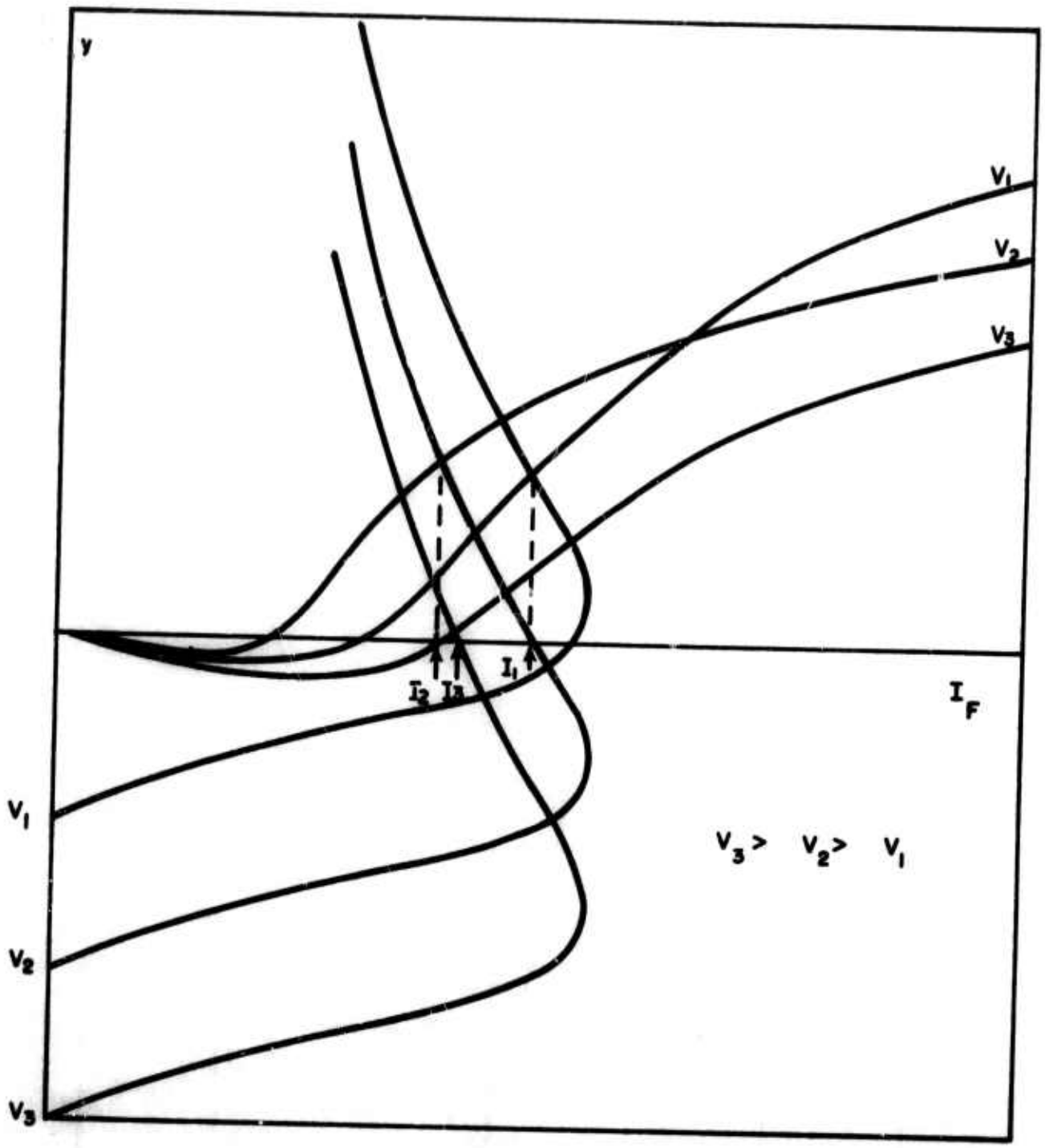

Figure 4. Network of Curves to Illustrate Properties of Solutions as V Increases

1-1930

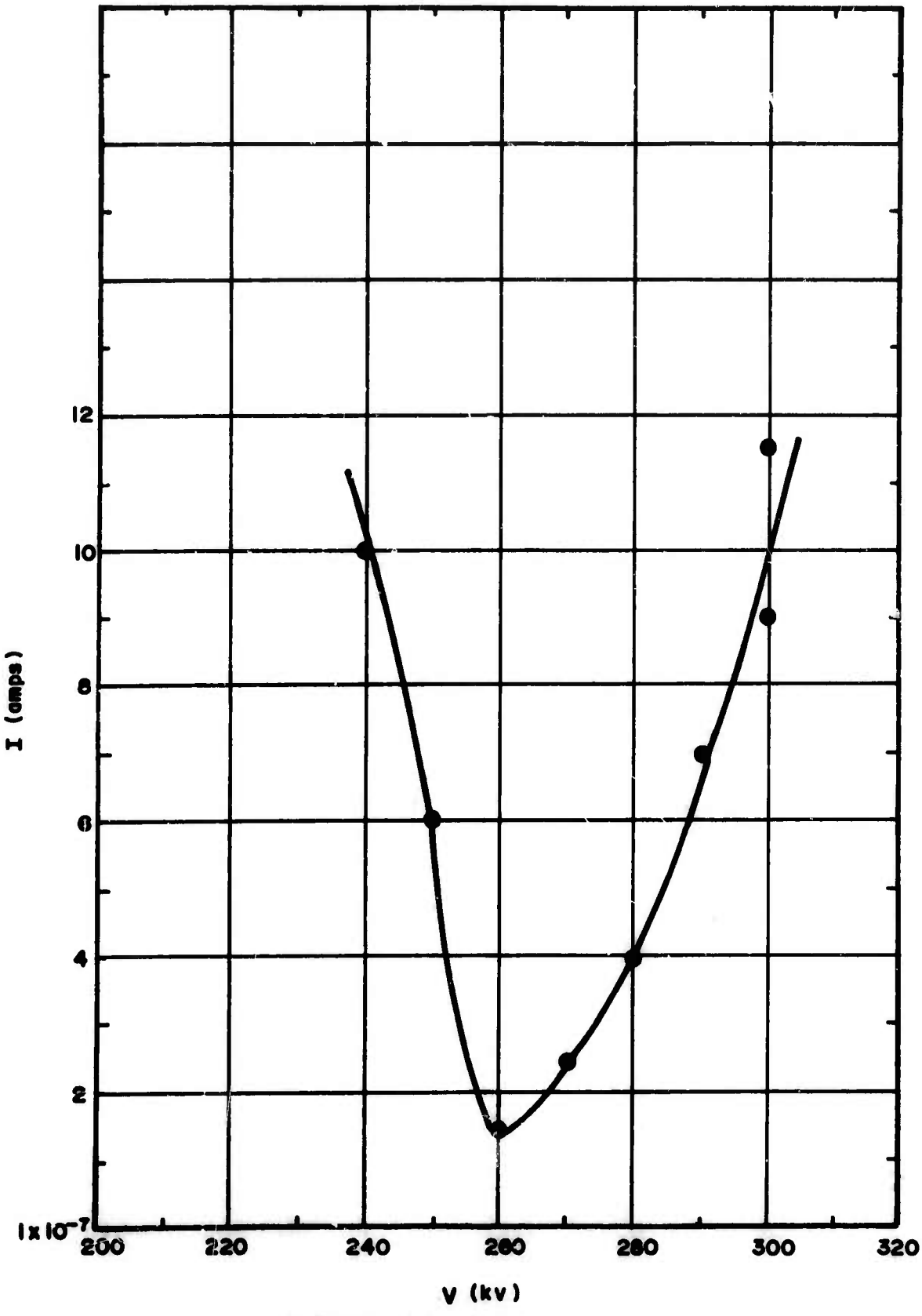

Figure 5. Current vs Voltage Showing Negative and Positive Slopes

2-542

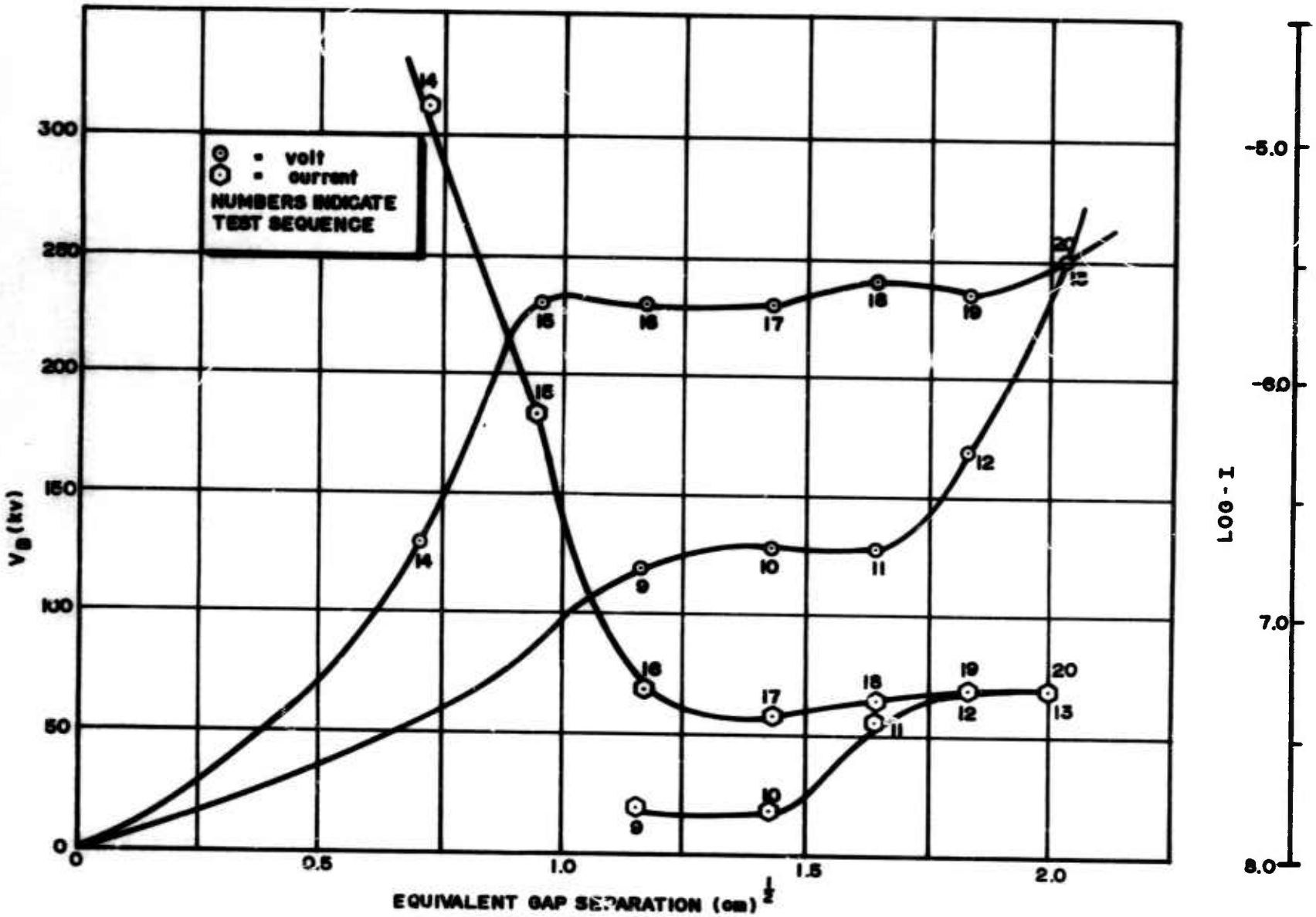

Figure 6. Breakdown Voltage and Prebreakdown Current as a Function of Gap Separation Showing Dual Breakdown Mode

4. STATISTICAL ANALYSIS

4.1 General

The pilot experiment has now been completed, and a preliminary statistical analysis carried out on the results. This was a seven factor, quarter replicate partial factorial experiment consisting of 32 treatments and 16 replications. For each treatment the unconditioned and conditioned breakdown parameters for 6 gaps in the range 0.5 to 3.0 cm were determined.

The statistical analysis initially was concentrated on the conditioned breakdown results. However before presenting this and discussing the trends, the objectives of the pilot experiment should again be borne in mind. Apart from investigation of the effects of the seven factors, these were familiarization with the apparatus and with the statistical technique, and finalization of a procedure which could be used for all future tests. In fact, the procedure described in this paper was not finalized until after about 12 treatments in the initial run had been completed. Within this frame of reference the analysis to date, has yielded the following.

4.2 Computer Program and Calculator Analysis

The program has as input, a set of 32 observations (e.g., 1.0 cm gap conditioned values of breakdown voltage) which has been set up in the "standard" order for Yates Algorithm described in ECOM 2655. The outputs of the program are given in two parts, the first being a printed evaluation of the contrast sums and coefficients for each of the terms of the mathematical model implied by the experimental design. This is complemented by a second printing in which these contrast sums and coefficients are ordered from largest to smallest absolute values (although the appropriate sign is retained in printing). The second part of the output is obtained after an arbitrary decision is made by the analyst as to the least magnitude worth retaining in the mathematical model. Having fixed this value, all smaller magnitudes are set to zero arbitrarily and this new input, (called X Prime in the printout is processed by the Reverse Yates Algorithm to estimate or "predict" observations comparable to the original input values. The difference between the "predicted" and observed value is given in the column headed "Residuals".

4.3 Analysis of Conditioned Breakdown Parameters

The analysis for the first 28 treatments was given in the previous Quarterly Progress Report. In fact, because of changes in procedure this only examined treatments 5 through 28. Also this analysis included both the unconditioned and conditioned breakdown values for the 1.0 gap.

The present analysis initially concentrated on the conditioned breakdown parameters for the 1.0 cm gap. The results were plotted on a half normal grid and the factors showing a significant influence (in order of rank) were A (anode material), E (anode geometry), B (cathode geometry), D (bakeout) and BC (of interactions of anode geometry with anode material and cathode geometry with cathode material).

The significance however, was insufficient to assign much reliability to the results and accordingly another method was used. The breakdown law:

$$V = Kd^{1/2}$$

was found to be approximately valid for breakdown voltages below 1.5 cm throughout the pilot experiment. In the second analysis the breakdown voltages at 0.5, 1.0 and 1.5 cm were used to compute an average value of K for this plot of Figure 7. The same factors were found to influence K but with much greater reliability. This of course is because three times as much data is employed.

A further analysis is planned using the formula:

$$VE_c = \text{constant}$$

where E_c is the calculated macroscopic surface yield at the cathode.

The purpose of this is to eliminate that part of the cathode geometry effect which is electrical in nature. It is expected to modify the contributions from B and BC and so to separate purely electrostatic geometry effects from any others operative.

4.4 Interpretation of Results

The most significant results of the experiment are the pronounced effects of the anode material, anode shape and cathode shape.

All of these factors play an important role in determining the value of the parameter gd^2/S appearing in Equation (28). From the physical standpoint this parameter is the product of factors g, determined by dissolved hydrogen concentration and diffusion coefficient of the material, and d^2/S which governs the capacity of the electrode geometry to disperse any gas evolved from the anode. Thus, curved electrodes have a higher pumping conductance than flat ones and gas is dispersed easily, requiring a higher applied voltage to generate enough gas to break down the gap.

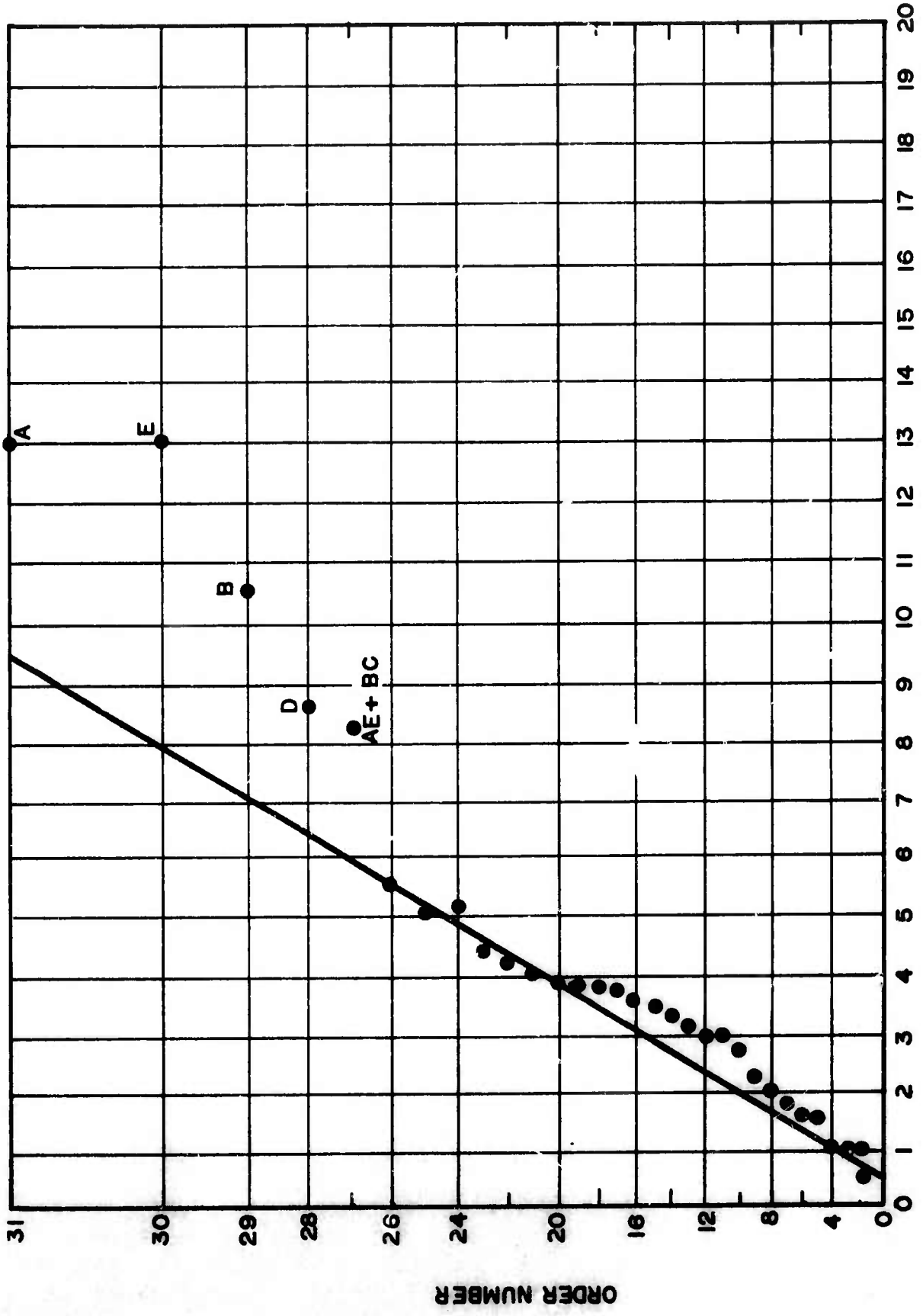

Figure 7. Semi-Normal Plot of the Results of the Pulse Experiment

2-544

The bakeout factor D shows that those treatments receiving both electrode and complete system bakeout have higher breakdown voltage than with only the electrodes baked out. This again supports the theoretical idea that bakeout reduces the dissolved hydrogen content and lowers the value of the gas supply parameter g.

4.5 Further Experimental Confirmation

A further statistical design is being prepared to confirm the theory that hydrogen in the anode is an undesirable factor in determining breakdown strength. Samples of copper will be treated at three levels of hydrogen content achieved by high temperature vacuum bakeout, no treatment at all, and high temperature hydrogen oven firing. In each case the electrodes will be baked out in the test chamber by the same treatment as previously. It is hoped that more widely varying geometry may also be tested at the same time. The result should be higher reliability in the trends and a definite indication of an interaction between gas concentration in the anode but not with the cathode.

5. FUTURE EFFORT

During the next quarter the following will be pursued:

- Statistical and physical analysis of the results of the pilot experiment will be continued.
- The first experiment of Phase II will be designed and initiated.
- The results will be tabulated and analyzed.
- Electrodes will be prepared, examined and photographed.
- The 300 kv system will be overhauled and maintained in an operational state.
- The magnetic field and energy storage systems will be checked out.
- Dielectric cylinders will be prepared for test.
- The electrode support structure and the baking system will be redesigned for ease and reliability of operation.

6. IDENTIFICATION OF PERSONNEL

The following personnel were active in the program during the period under review:

A. S. Denholm	- Department Manager
M. J. Mulcahy	- Project Manager
A. C. Stewart	- Engineering Manager
G. K. Simcox	- Electrical Engineer
M. M. Thayer	- Metallurgist
A. Watson	- Physicist
R. M. Parsons	- Engineering Aide
L. Silva	- Design Engineer
C. Boudreau	- Engineering Aide
F. Battistello	- Technician
L. Andingaro	- Metallurgical Technician
Prof. H. Freeman	- Consultant MIT, Department of Economics and Social Science
Prof. A. Argon	- Consultant MIT, Department of Mechanical Engineering
Dr. N. E. Woldman	- Consultant Metallurgy

7. REFERENCES

(1) Chatterton, P. A., Proc. Phys. Soc., 88, 231 (1966).

(2) Rose, D. J. and Clark, M. Jr., "Plasmas and Controlled Fusion" M. I. T. Press and Wiley, (1966).

APPENDIX 1

INTEGRATION OF POISSON'S EQUATION

INTEGRATION OF POISSON'S EQUATION

The electric field strength X_s, at the cathode surface due to positive and negative space charge accumulation can be derived by integration of Poisson's equation. Studying it in one dimension for simplicity we have:

$$\frac{d^2U}{dx^2} \equiv \frac{d}{dn}\left(\frac{dn}{dx}\right)^2 = \left(n_+ - n_e\right) e = \frac{J_+}{v_+} - \frac{J_e}{v_e} \qquad \text{(A1-1)}$$

When the mean free path of ions and electrons is greater than the electrode gap separation they will accelerate freely in the electric field and hence:

$$v_+ = \sqrt{\frac{2e}{m_+}}$$

$$v_e = \sqrt{\frac{2e}{m_e}} \qquad \text{(A1-2)}$$

where m_+, me are the masses of ions and electrons respectively.

Hence for a flow of electrons and ions streaming against one another Poisson's equation reduces to:

$$\frac{d}{dn}\left(\frac{dn}{dx}\right)^2 = \frac{J_e}{\sqrt{\frac{2e}{m_e}}} \cdot \frac{1}{\sqrt{U}} \cdot \left[\frac{J_+}{J_e}\sqrt{\frac{m_+}{m_e}} - 1\right] \qquad \text{(A1-3)}$$

This will integrate readily for constant values of current density to yield the familiar form known as McKeown's equation[1]. In the case under consideration however, the current densities are not constant throughout the gap although it is assumed that their rato is when J_e and J_+ are created within the

same volume. The majority of the total electron current however is provided by field emission and must be accounted for by an extra term:

$$\frac{d}{dU}\left(\frac{dU}{dx}\right)^2 = \sqrt{\frac{J_+}{\frac{2eU}{m_+}}} - \sqrt{\frac{J_e}{\frac{2eU}{m_e}}} - \sqrt{\frac{J_F}{\frac{2eU}{m_e}}} \qquad \text{(A1-4)}$$

Care must be exercised in integrating this equation when J_+ and J_e are considered as being created continuously within the volume of the primary beam I_F. Consider the ionization current created in a section of the beam at potential U as in Figure A1-1. The increment of rate of ionization is:

$$\frac{dN_+}{dt} \doteq J_F N \frac{\sigma_o}{U} dx \qquad \text{(A1-5)}$$

and since all ion generation is assumed to be collected by the electrodes then:

$$J_+ = \frac{dN_+}{dt} .$$

The total ion current is hence:

$$\begin{aligned} J_+ &= J_F N \sigma_o \int \frac{dx}{U} \\ &= J_F N \sigma_o \int \frac{dU}{U\left(\frac{dU}{dx}\right)} \end{aligned} \qquad \text{(A1-6)}$$

The value of $\frac{dU}{dx}$ is a strong function of position only close to the emitting tip and this region is outside the region of ionization so it can be neglected and a uniform field of V/d assumed. Hence:

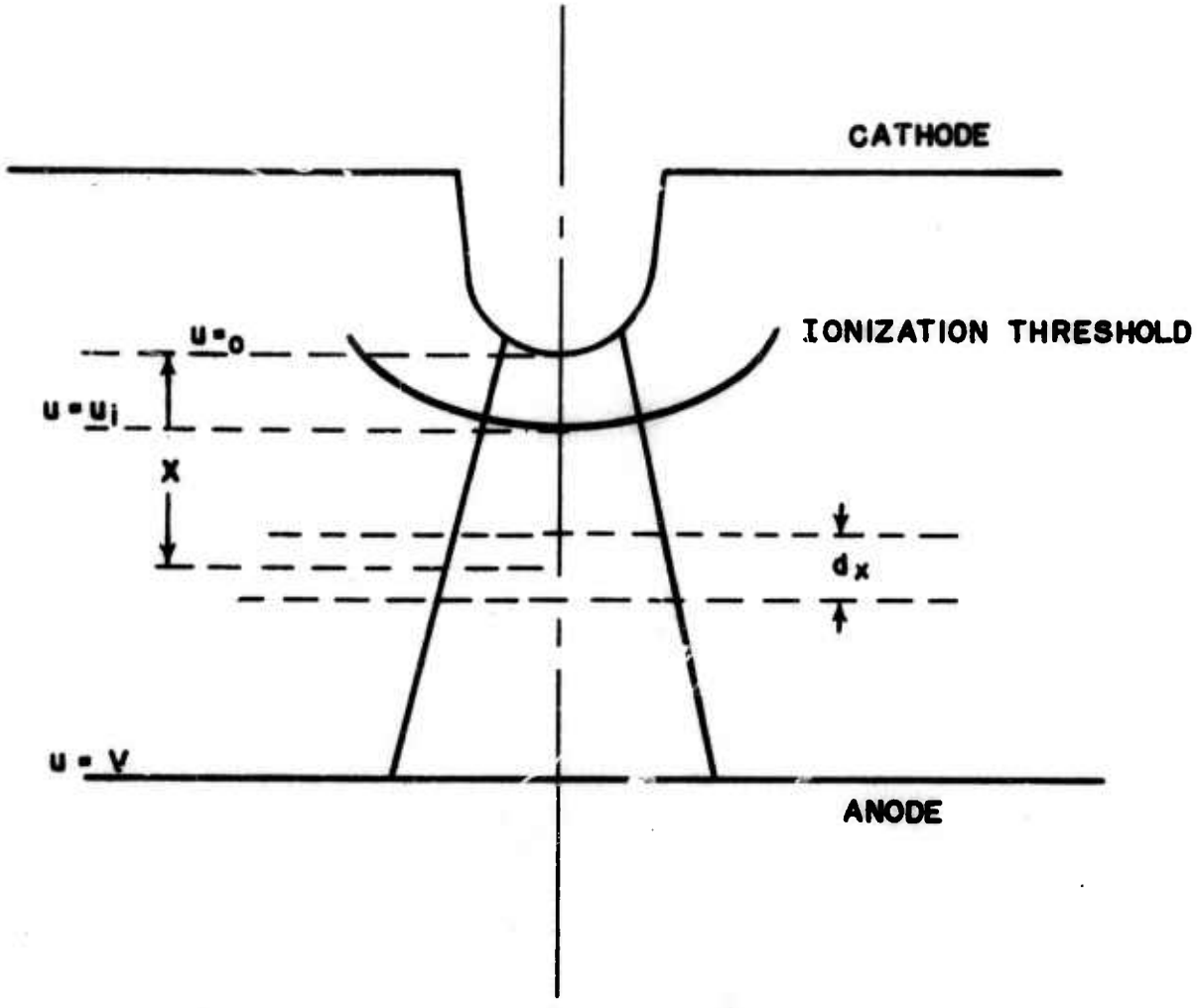

Figure A1-1. Diagram to Illustrate the Ionization Process in the Interelectrode Space

$$J_+ = \frac{J_F N \sigma_o d}{V} \int_{U_i}^{V} \frac{dU}{U} \qquad (A1\text{-}7)$$

$$= \frac{J_F N \sigma_o d}{V} \ln \left(\frac{V}{U_i} \right)$$

where U_i is the ionization potential. Although the ion current is integrated in this manner each increment at potential U will contribute to $\left(\frac{dU}{dx} \right)_s$ and we have from Equation (A1-4)

$$\left| J_+ \right| = \left| J_e \right|$$

$$\therefore \frac{d}{dU} \left(\frac{dU}{dx} \right)^2 = \frac{J_e}{\sqrt{\frac{2e}{m_e}}} \frac{1}{\sqrt{U}} (\mu - 1) \qquad (A1\text{-}8)$$

where

$$\mu \equiv \sqrt{\frac{m_+}{m_e}}$$

and since J_e is weighted according to the value of U at which ionization occurred then:

$$\frac{d}{dU} \left(\frac{dU}{dx} \right)^2 = \frac{J_F N \sigma_o d}{V \sqrt{\frac{2e}{m_e}}} \frac{(\mu - 1)}{U \sqrt{U}} \qquad (A1\text{-}9)$$

Integrating this we have:

$$\left(\frac{dU}{dx}\right)^2 = \frac{J_F N \sigma_o (\mu - 1) d}{V\sqrt{\frac{2e}{m_e}}} \int_{U_i}^{V} \frac{dU}{U^{3/2}} \tag{A1-10}$$

$$= \frac{J_F N \sigma_o (\mu - 1) d}{V\sqrt{\frac{2e}{m_e}}} \left[\frac{2}{3} \left(\frac{1}{\sqrt{U_i}} - \frac{1}{V} \right) \right]$$

Since $U_i \ll V$ the second limit can be neglected and

$$\left(\frac{dU}{dx}\right)^2 = \frac{2 J_F N \sigma_o (\mu - 1) d}{3V\sqrt{\frac{2eU_i}{m_e}}} \tag{A1-11}$$

So far we have not considered the third term in Equation (4). When it is included and integrated we have:

$$X_s^2 \equiv \left(\frac{dU}{dx}\right)_s^2 = \frac{2 J_F N \sigma_o (\mu - 1) d}{3V\sqrt{\frac{2eU_i}{m_e}}} - \int_o^V \frac{J_F}{\sqrt{\frac{2eU}{m_e}}} \tag{A1-12}$$

$$= \frac{J_F \sqrt{V}}{\sqrt{\frac{2e}{m_e}}} \left[\frac{2N \sigma_o (\mu - 1) d}{V^{3/2}\sqrt{U_i}} - 1 \right]$$

In this final integration the initial exit velocity of the electrons by field emission has been neglected. This has been treated by Stern, Gossling and Fowler[2] and is a valid approximation at very high current densities, such as would be expected close to the breakdown condition.

REFERENCES

(1) McKeown, S.S., Phys. Rev., 34, 611 (1929).

(2) Stern, T.E., Gossling, S.L. and Fowler, R.H., Proc. Roy. Soc., (London) Series A, 124, (1929).

APPENDIX 2

RATE OF GAS EVOLUTION FROM THE ANODE

RATE OF GAS EVOLUTION FROM THE ANODE

Temperature and density profiles governed respectively by the diffusion of thermal energy by conduction or by matter transport according to Fick's law follow the same basic partial differential equations.

$$\left.\begin{aligned} K \nabla T &= P \\ D \nabla n &= \dot{n} \end{aligned}\right\} \qquad \text{(A2-1)}$$

The difference lies in D(T) which is a function of temperature and, therefore, of position.

The geometry of each diffusion process is identical and the boundary conditions are similar if it is assumed that gas is evolved only from the heated disc surface and negligibly from the surrounding part of the surface. The gradients are opposite since mass transport is towards the surface and heat transfer $P/cm^2/sec$ away from it (Fig. A2-1). Hence, consider the total rate of particle transport $\dot{N}/cm^2/sec$ to be a mass flow directed opposite to the heat flow. Thus:

$$\frac{D(T)\,\nabla n}{K \nabla T} = \frac{\dot{N}}{P} \qquad \text{(A2-2)}$$

if steady state conditions are assumed.

$$\therefore \frac{\nabla n}{\nabla T} \equiv \frac{dn}{dT} \equiv \frac{\dot{N}K}{PD(T)} \qquad \text{(A2-3)}$$

This equation shows that for an identical displacement the incremental change of number density with temperature is a function of temperature. Thus the number density difference between the surface and deeply inside the surface is obtained by integration of this between the corresponding temperature limits (Figure A2-2).

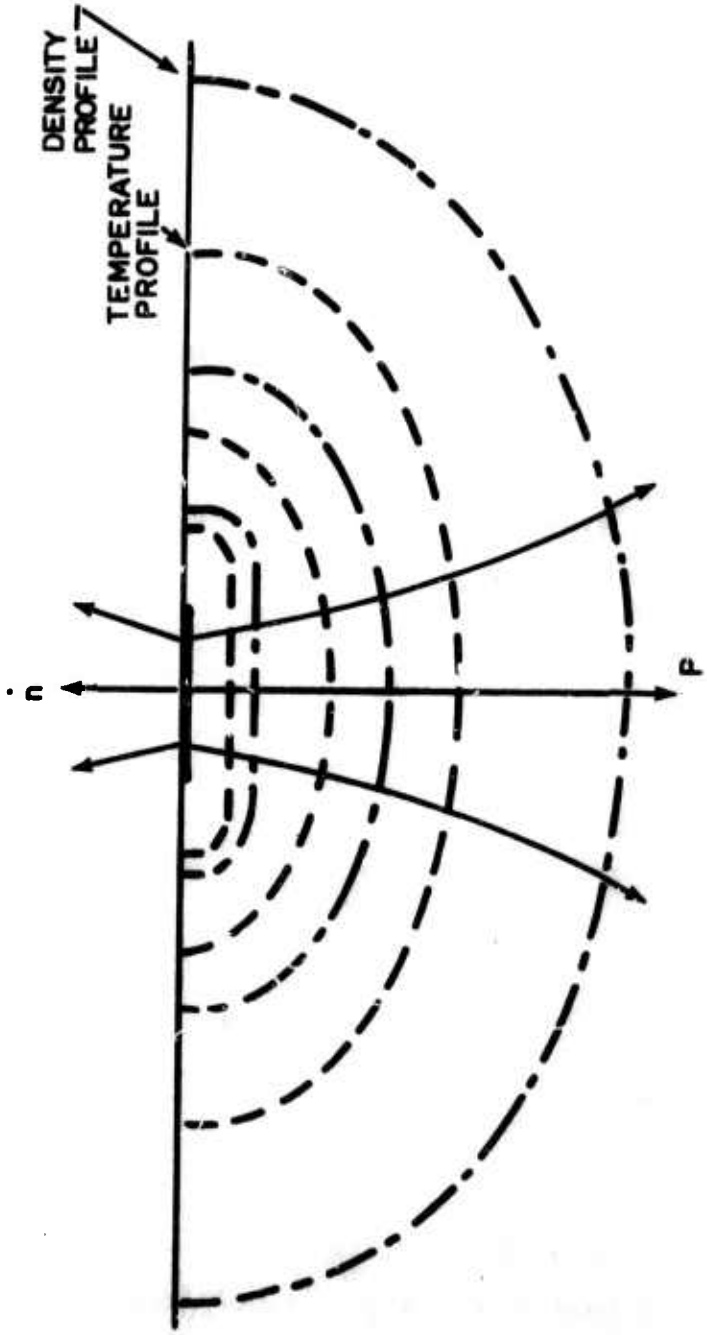

Figure A2-1. Anode Temperature and Gas Density Profiles Beneath a Hot Spot

2-546

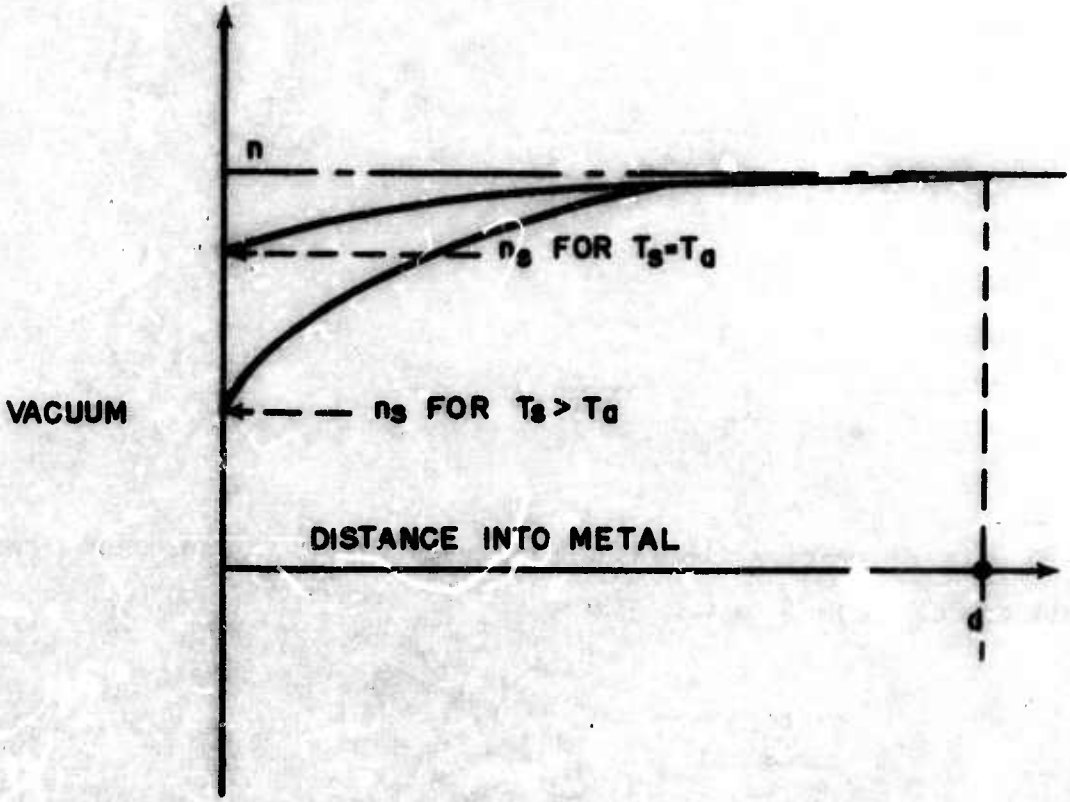

Figure A2-2. Gas Density Distribution Beneath Metal Surface

$$\int_{n}^{n_s} dn = \frac{\dot{N}}{P} \int_{T_a}^{T_s} \frac{dT}{D(T)} \qquad \text{(A2-4)}$$

But

$$W = IV = 4KR\,(T_s - T_a) = \pi R^2 P \qquad \text{(A2-5)}$$

$$\therefore \quad n_s - n = \frac{\dot{N}}{4R(T_s - T_a)} \int_{T_a}^{T_s} \frac{dT}{D(T)} \qquad \text{(A2-6)}$$

and

$$\frac{1}{T_s - T_a} \int_{T_a}^{T_s} \frac{dT}{D(T)} = \overline{D^{-1}} \qquad \text{(A2-7)}$$

where $\overline{D^{-1}}$ is the average value of the inverse of the diffusion coefficient between the surface and the bulk metal. Thus,

$$n - n_s = \frac{\dot{N}}{4R}\ \overline{D^{-1}} \qquad \text{(A2-8)}$$

The rate of gas evolution can now be calculated from the rate $\dot{n}$ per cm^2/sec at which the surface atoms surmount the surface energy barrier h_s.

The number density of atoms at the surface, n_s has just been shown to be related to the rate of evaporation from the surface $\dot{N}$ by the diffusion process. Gas atoms present at the surface must acquire an activation energy h_s to leave the metal as well as the energy H to diffuse. Hence, the number leaving the surface will be equal to the rate of arrival from inside the metal multiplied by the Boltzmann factor:

$$\exp\left(-\frac{h_s}{kT_s}\right).$$

Thus the number of unbound atoms will be $n_s \exp\left(-\frac{H}{kT_s}\right)$ and the arrival rate will be $\frac{n_s\bar{c}}{4}$ so the number leaving the surface per unit area/sec

$$= \frac{n_s\bar{c}}{4} \exp\left\{-\frac{H + h_s}{kT_s}\right\} \tag{A2-9}$$

where $\bar{c}$ is the most probable thermal velocity. Thus the total number $\dot{N}$ is

$$\dot{N} = \pi R^2 \frac{n_s\bar{c}}{4} \exp\left\{-\frac{H + h_s}{kT_s}\right\}$$

$$= \left\{n - \frac{\dot{N}}{4R}\overline{D^{-1}}\right\} \frac{\pi R^2\bar{c}}{4} \exp\left\{-\frac{H + h_s}{kT_s}\right\} \tag{A2-10}$$

$$\frac{n}{\dot{N}} - \frac{\overline{D^{-1}}}{4R} = \frac{4}{\pi R^2\bar{c}} \exp\left\{\frac{H + h_s}{kT_s}\right\} \tag{A2-11}$$

$$\frac{n}{\dot{N}} = \frac{\overline{D^{-1}}}{4R} + \frac{4}{\pi R^2\bar{c}} \exp\left\{\frac{H + h_s}{kT_s}\right\}$$

and

$$\dot{N} = \frac{n}{\frac{\overline{D^{-1}}}{4R} + \frac{4}{\pi R^2\bar{c}} \exp\left\{\frac{H + h_s}{kT_s}\right\}} \tag{A2-12}$$

and

$$\overline{D^{-1}} = \frac{1}{D_o} \exp\left\{\frac{H}{kT_m}\right\} \tag{A2-13}$$

where T_m is a weighted mean temperature (Figure A2-3).

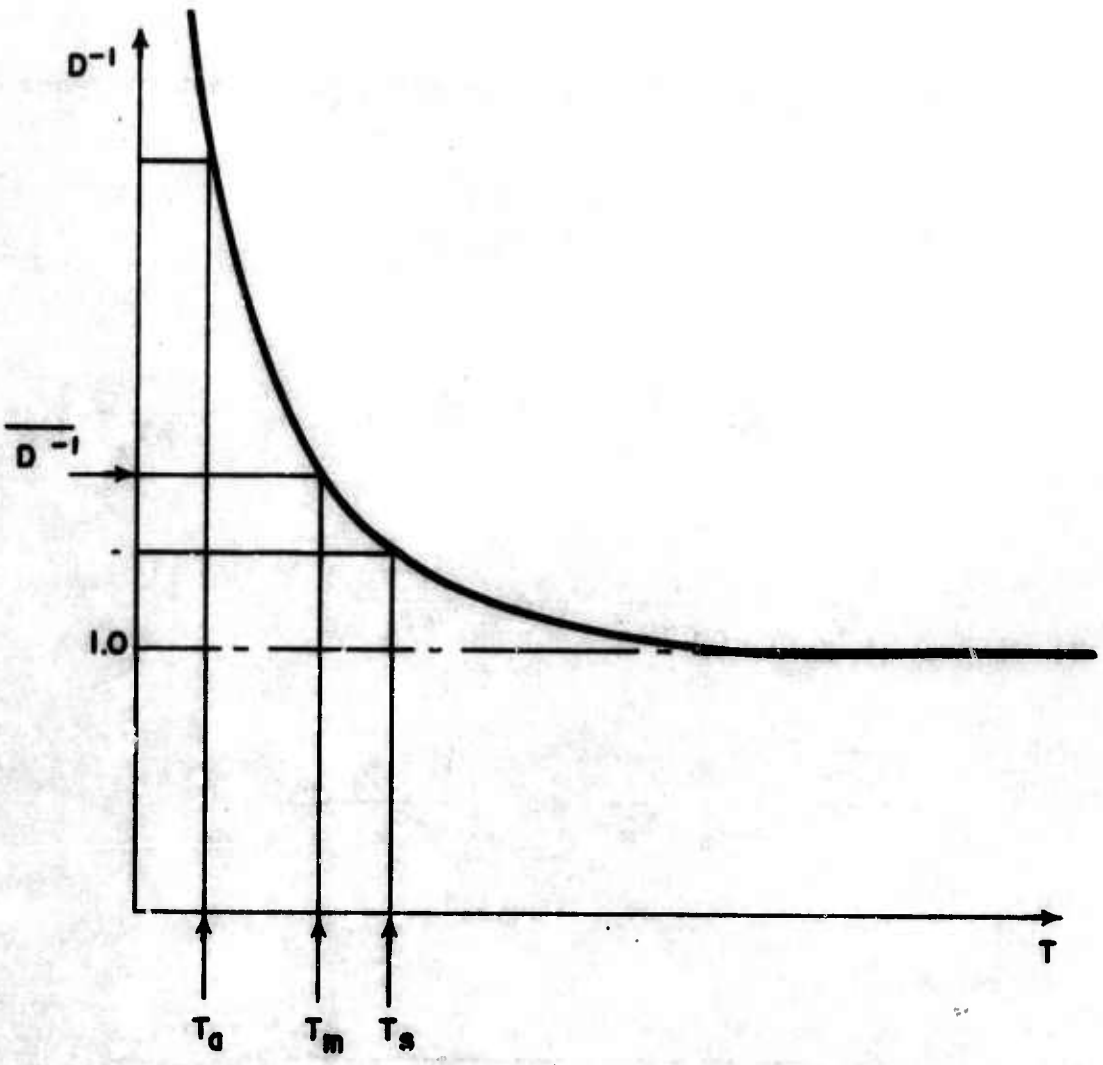

Figure A2-3. Illustration of Inverse of the Diffusion Coefficient as a Function of Temperature

$$\dot{N} = \frac{n}{\frac{1}{4RD_o} \exp\left(\frac{H}{kT_m}\right) + \frac{4}{\pi R^2 \bar{c}} \exp\left\{\frac{H + h_s}{kT_s}\right\}} \qquad \text{(A2-14)}$$

$$T_m = T_s \left(\frac{T_m}{T_s}\right)$$

$$\therefore \dot{N} = \frac{n \exp\left(-\frac{H}{kT_s}\right)}{\frac{1}{4RD_o} \exp\left\{\frac{H}{k}\left(\frac{1}{T_m} - \frac{1}{T_s}\right)\right\} + \frac{4}{\pi R^2 \bar{c}} \exp\left\{\frac{h_s}{kT_s}\right\}} \qquad \text{(A2-15)}$$

$$\bar{c} = \sqrt{\frac{3kT_s}{8\pi_M}}$$

When the second term in the denominator is dominant we have:

$$\dot{N} \sim \pi R^2 \frac{n\bar{c}}{4} \exp\left\{-\frac{H + h_s}{kT_s}\right\} = \frac{\pi R^2}{4} \sqrt{\frac{3kT_s}{8\pi_m}}\, n \exp\left\{-\frac{H + h_s}{kT_s}\right\} \qquad \text{(A2-16)}$$

From the density profile it is seen that $n_s \approx n$ and the surface depletion is small i.e., when the rate of evaporation is relatively small.

When the first term is dominant we have:

$$\dot{N} \doteq 4RD_o\, n \exp\left(-\frac{H}{kT_m}\right) \qquad \text{(A2-17)}$$

APPENDIX 3

THE PUMPING CONDUCTANCE OF PLANE PARALLEL DISCS

THE PUMPING CONDUCTANCE OF PLANE PARALLEL DISCS

The streaming of a gas down a tube results from a density gradient of molecules between its extremities. A similar argument applies of course between the axis and periphery of two plane parallel electrodes when gas is evolved at the center of one electrode. Molecules collide with the solid surfaces, losing momentum and being scattered in random directions. There will thus be a resultant molecular flow only when there is a greater density of molecules at one place than at another. This difference in number density can then be related to the rate of flow of gas through the system.

There is a relationship between the mass flow M and pressure gradient dp/dl across any vacuum pumping impedance.[1]

$$M = -\left(\frac{8}{3}\sqrt{\frac{2}{\pi}}\right)\sqrt{\rho_1}\,\frac{A^2}{O}\,\frac{dp}{dl} \qquad \text{(A3-1)}$$

where

A = area of cross section

O = circumference of normal cross section.

For two discs of radius a separated by a gap d we have:

$$A = 2\pi rd$$
$$O = 2 \times 2\pi r = 4\pi r \qquad \text{(A3-2)}$$
$$\frac{A^2}{O} = \pi r d^2$$

and

$$\frac{dp}{dl} = \frac{dp}{dr} \qquad \text{(A3-3)}$$

$$\therefore M = -\left(\frac{8}{3}\sqrt{\frac{2}{\pi}}\right)\sqrt{\rho_1}\ \pi d^2\ \frac{dp}{d(\ln r)} = -K\ \frac{dp}{d(\ln r)} \qquad \text{(A3-4)}$$

Integrating between any radius r and the periphery we have:

$$\frac{M}{K}\ \ln\left(\frac{P}{a}\right) = p_a - p_R = \Delta p. \qquad \text{(A3-5)}$$

But:

$$M = m\dot{N} \qquad \text{(A3-6)}$$

and:

$$\Delta p = \Delta N\ (kT) \qquad \text{(A3-7)}$$

$$\therefore \dot{N} = -\Delta N\left(\frac{kT}{m}\right)\left[\frac{8}{3}\sqrt{\frac{2}{\pi}}\right]\sqrt{\rho_1}\ \pi d^2\ \ln\left(\frac{R}{a}\right) \qquad \text{(A3-8)}$$

Hence the pumping conductance is:

$$S = -\frac{\dot{N}}{\Delta N}$$

$$= \left(\frac{kT}{m}\right)\sqrt{\rho_1}\left[\frac{8}{3}\sqrt{2\pi}\right]d^2\ \ln\left(\frac{R}{a}\right) \qquad \text{(A3-9)}$$

where

R = radius of hot spot
a = radius of electrode
T = gas temperature
ρ = density at temperature of experiment and at 1 dyne/cm^2 pressure.
d = gap separation

The rate of gas flow has thus far been arbitrarily chosen. It can be related to the value $\dot{N}$ of gas evolved from an anode hot spot by considering the fraction intercepted by the cathode. Only this portion can take part in the streaming, the remainder being lost to the pump as fast as it is evolved. The angular distribution of the evolved molecules will be according to cos θ where θ is the angle between the molecular velocity and the normal. Hence the fraction intercepted by the cathode is:

$$\frac{\int_0^{\tan^{-1}\left(\frac{a}{d}\right)} \cos\theta \, d\theta}{\int_0^{\pi/2} \cos\theta \, d\theta}$$

$$= \frac{a}{\sqrt{a^2 + d^2}} \qquad \text{(A3-10)}$$

This factor will multiply the pumping conductance. Therefore:

$$S = \frac{a}{\sqrt{a^2 + d^2}} \cdot \frac{\dot{N}}{\Delta N} \cdot \qquad \text{(A3-11)}$$

$$S = \left[\frac{8}{3}\sqrt{2\pi}\right]\left(\frac{kT}{m}\right) \rho_1 \frac{ad^2}{\sqrt{a^2 + d^2}} \cdot \ln\left(\frac{R}{a}\right) \qquad \text{(A3-12)}$$

REFERENCES

(1) Roberts, J.K. and Miller, A.R., "Heat and Thermodynamics" Chapter 3, (Blackie, 1951).

APPENDIX 4

PREBREAKDOWN PHENOMENA IN VACUUM GAPS

PREBREAKDOWN PHENOMENA IN VACUUM GAPS

by

A. Watson, A. S. Denholm and M. J. Mulcahy
Ion Physics Corporation

INTRODUCTION

A characteristic of electrode gaps in vacuum is that there exists no unique breakdown voltage but only a band of possible values attainable after many prior sparks have passed during an initial "conditioning" procedure. The literature to date is confused about the significance of this procedure and of the electrode materials, shapes and finish in determining breakdown voltage. It is pertinent to question whether shape and finish, which are disturbed after sparking, can be preserved by a different choice of procedure for voltage application, leaving them available for the experimenter to vary at will.

It should be theoretically possible to monitor enough physical variables during voltage application to describe adequately the processes leading up to gap failure. Recognition of an incipient breakdown without damaging the electrodes would permit repetitive testing under similar conditions, being particularly useful with low impedance power supplies.

The present investigation was directed towards developing a conditioning procedure involving minimal sparking and to search for a criterion for incipient breakdown.

One shape only of large area, unbaked, metallurgically polished stainless steel electrodes was used throughout. During stepwise voltage application the variables monitored were gap current, light output, partial pressure of hydrogen or nitrogen, and X-radiation. The processes accompanying the approach to gap failure were thus monitored, to see if they were slow enough to permit recognition of a breakdown criterion.

APPARATUS

Hollow domes of 304 stainless steel serving as approximately uniform field electrodes, 8 inches in diameter, were centrally positioned at fixed gaps of up to 1 cm within the 3 foot wide stainless steel vacuum chamber at the ends of two 250 kv bushings. Organic contamination was eliminated by using gold gaskets throughout, and pumping down to 6.10^{-7} torr with a mercury diffusion pump and liquid nitrogen cold trap. The mass spectrometer ion source, protruding inside from the wall was screened from the large applied field within the chamber which otherwise perturbed it. Outside of the 3/4 inch thick glass monitoring port were two thallium activated NaI scintillators viewing, respectively, either the whole electrode region or only the inter-electrode space through a collimator made from two narrowly separated

parallel aluminum slabs. Visible radiation from this port was reflected sideways by a plane mirror to a photomultiplier to separate it from accompanying X-radiation, thus avoiding damage to the photocathode.

Gap current fluctuations were observed using a 160 kv, 1.5 mA rectifier source and external resistors of 400 kilohm and 15 megohm to vary the effective output impedance.

The electrodes were hand ground initially with wet silicon carbide paper of successively finer grade, followed by finer grinding on a variable speed wheel. This was continued with silk using a succession of fine grades of alumina powder and was completed with a wash and wipedown with gamal cloth.

ELECTRODE CONDITIONING

Starting with fresh unconditioned electrodes the voltage was increased in steps of 2, 5 or 10 kv, depending on the gap setting and the voltage, while at the same time monitoring the N_2 or H_2 partial pressure peak on the mass spectrometer. It was found, by observing the current pulse shapes and the associated partial pressure rises that a threshold voltage existed for the appearance of microdischarges. A plot of initial threshold voltage versus gap separation is shown in Figure 1. This is in good agreement with a similar plot of Arnal.[1] Microdischarges appeared as groups of apparently damped oscillatory waveforms similar to those described by Mansfield et al[2] and associated with X-radiation pulses modulated in frequency according to the pressure rise (Figure 3).

During the course of the microdischarge investigation no pressure increases were observed until the microdischarge threshold voltage was reached, and above this the magnitude increased with the height of the voltage steps. Frequent breakdowns occurred when the pressure increases were large and it was found that these could be reduced in number, if not eliminated, by using smaller voltage steps. Occasionally large pressure increases did occur, in which case the voltage was reduced or switched off before breakdown could take place.

From these observations a conditioning procedure was evolved for unbaked but clean polished electrode surfaces. Initially the voltage was increased incrementally every two minutes until a pressure rise was observed, and then allowed to decay to zero. The height of the voltage steps was limited to a level at which breakdowns were unlikely to occur during the gas surge and the stepwise voltage increase was continued until surface roughening took place (to be described later).

The conditioning apparently involves the controlled removal of gas from the electrodes.

Comparison in Figure 2 of the breakdown voltages measured with the new technique and with spark conditioning clearly shows improvement in the breakdown voltage and its deterioration as a function of number of sparks.

MONITORING TECHNIQUES

Pulse height histograms drawn from scintillator signal oscillograms of microdischarge activity showed that during the pressure surge there were two peaks in the photon energy spectrum (Figure 4) but after its decay the lower energy peak disappeared. Microdischarge current, although initiated by an ion exchange mechanism, was shown by Mansfield[2] and Pivovar and Gordienko[3] to be mostly electrons. The anode presents a thick absorbing X-ray target to these, most of which assume the whole applied potential but during the pressure surge, interelectrode gas intervenes as an additional thin target, intercepting some electrons to generate the lower photon energy peak.

When high voltages were reached with the new conditioning procedure a steady X-radiation level grew due to cold cathode Fowler-Nordheim emission from sites of enhanced field strength just as Pivovar and Gordienko[3] have observed and attributed to surface etching. At still higher voltages the level rose while microdischarges abated, permitting an accurate measurement of the steady X-ray level as a function of voltage. Typical recordings are shown in Figure 5.

In thick targets, electrons generate X-radiation intensity U_x proportionally to the square of the applied voltage, V.[4] Hence relative changes in electron current can be derived from corresponding X-radiation densities and this technique has been used throughout the present investigation. Electrons emitted according to the Fowler-Nordheim law thus produce X-radiation according to:

$$U_x = A K \frac{\beta^2 V^4}{d^2} \exp\left(- \frac{Bd}{\beta V}\right) \qquad (1)$$

where:

B, K = constants
A = emitting area
d = gap separation
β = field enhancement factor

A plot of log (U_x/V^4) as a function of V^{-1} should thus be linear.

Without measured work functions these plots yield only relative values of field enhancement factor and emitting area but their present value is in signifying changes in these parameters taking place as breakdown is approached. While linear plots occurred in this investigation, the commoner non-linear variety (Figure 6) evidenced cathode surface changes as the voltage increased. Repetitively raising and lowering the voltage in increments without sparking failed to yield reproducible results (Figure 7). When extended to the breakdown limit this procedure failed to show any correlation between the penultimate field enhancement factor and breakdown voltage (Figure 8).

Emission parameters, being derived from the slope of the Fowler-Nordheim plot, require readings at several voltage levels for their measurement. When they are time dependent the parameter changes should be small during the interval between voltage increments to permit approximate measurement. As breakdown approached the changes grew faster and rendered their measurement impossible. Changes in field enhancement factor and emitting area were occurring at constant voltage.

Gas or vapor evolution rate just prior to breakdown then suggested itself as a potentially significant parameter with which to describe the approaching breakdown since the accompanying X-ray emission is readily detectable in the case of microdischarges. Radiation density U_{xc} from the interelectrode space is proportional to the product of gas density, n_g, electron current I_e and the Bremsstrahlung cross section σ_B.[4]

U_{xc} was accordingly monitored by directing at the interelectrode space a collimator made from two narrowly separated aluminum slabs through which photons passed to a scintillator. The current was simultaneously monitored and the relative gas density was derived from:

$$n_g = \frac{U_{xc}}{I_e \sigma_B} \tag{2}$$

$$\sigma_B = \frac{8}{3\pi} \cdot \frac{1}{137} \cdot Z^2 \cdot \frac{c^2}{v^2} \doteq K Z^2 V^{-1} \tag{3}$$

where K = constant. Hence:

$$n_g = \frac{U_{xc} V}{K I_e Z^2} \tag{4}$$

A typical recording appears in Figure 9.

The right hand side of Equation (4) was evaluated experimentally and is plotted in Figure 10 as a function of voltage up to breakdown. Surprisingly the gas density appears to decrease but the illusion is dispelled by noting that σ_B can decrease if the interelectrode gas is progressively diluted with hydrogen. This would reduce the mean square cross section and produce the observed effect if n_g does not increase too much. Evidence of this was gathered from hydrogen partial pressure records from the mass spectrometer which shows surges as breakdown is approached. It thus appears that hydrogen gas accumulates in the gap.

Light intensity was monitored under these conditions as it increased stepwise with voltage together with X-ray intensity (Figure 11). At higher voltages both X-radiation and light output rose at constant voltage as well as the light output per unit current. Since the light growth occurs during the gas evolution phase it seems most likely due to gas luminescence. Transition

radiation would also appear but it cannot explain the increase in light output per unit current which would have to remain fixed at constant voltage.

This gradual increase at constant voltage of all of the measured parameters, total and collimated X-radiation, hydrogen partial pressure and light output was found to increase steadily during the last few voltage increments of 1 kv or less prior to breakdown. The phenomenon has been termed "runaway".

Reduction of the voltage by up to 10% was found to be insufficient to arrest this regenerative process which may take many seconds to complete (see Figure 12, the apparent fall in X-ray level is due to scintillator saturation). Breakdown voltages were very reproducible when voltage was applied in 5, 10 or 25 second intervals but a conditioning effect took place. Experiments with 2.5 mm and 5 mm gaps established that the breakdown voltage varies as the square root of the gap separation.

CONCLUSIONS

From this work it appears that only under restricted conditions is there a nondestructive criterion for incipient breakdown of vacuum gaps. Nonetheless the techniques developed and enumerated below are of value in permitting the vacuum gap to be completely described prior to and during breakdown. Thus, current or total X-radiation monitoring each give information on the state of the cathode surface and on microdischarge activity. Collimated X-radiation gives the total residual gas or vapor pressure in the gap with a rapid response time and is complemented by mass spectrometry which yields only chamber pressure but can resolve gas constituents. A steady uncontrolled runaway is indicated by the total and collimated X-radiation measurements under restricted conditions. This is further supported by visible radiation monitoring which is extremely sensitive to the effect.

In conclusion the preliminary program has been successful in yielding data from which the steps leading up to breakdown have been identified. Prebreakdown phenomena associated only with unbaked electrodes have been studied and the principal conclusions derived from this program can be summarized as follows:

1. A conditioning technique has been developed which does not involve sparking and consequent electrode damage. The technique has been compared with the more conventional spark conditioning method and the decrease in gap strength by sparking has been measured.

2. Microdischarge phenomena have been studied and the results largely verify the work of previous investigators. In addition, an associated rise in the partial pressures of residual gases has been studied.

3. Microdischarge activity has been shown to be followed by a field enhancement at the cathode and the consequent Fowler-Nordheim field emission probably occurs from a variety of sites. Discontinuities in

current changes as a function of voltage are believed to be due to the disappearance or reshaping of some sites.

4. X-rays are produced by microdischarges and by field emitted electrons. Photons can be generated in the gas or vapor released into the interelectrode space as well as from the anode as a target. The X-rays produced by field emission yield equivalent Fowler-Nordheim plots.

5. At high potentials the enhancement factor grows at constant voltage and can run away to breakdown. Small reductions of voltage will only decay the breakdown after growth has proceeded.

6. The visible radiation from the gap is consistent with a model in which transition radiation may appear at low currents but gas luminescence seems significant at runaway.

7. Monitoring by collimated X-radiation and mass spectrometry shows that there are both pulsed and continuous changes in interelectrode gas density prior to breakdown. The gas appears to be hydrogen which probably diffuses out from the anode when it is heated sufficiently by electron bombardment.

8. Gap failure can occur under two apparently separate circumstances: (a) when gas pressure rises due to microdischarges become too great, (b) after surface etching and the runaway of the field enhancement factor. In case (b) the buildup of hydrogen density in the gap may also be the cause of breakdown since it seems to be always associated with it.

9. The breakdown voltages at runaway are consistent and the conditioned breakdown voltages appear to be approximately proportional to the square root of the gap separation.

ACKNOWLEDGMENTS

The authors gratefully extend their thanks to R. Parsons for his work in assembling the equipment and performing the experiments, and to M. M. Thayer, R. Parsons and L. Ingingaro for their assistance.

This work was sponsored by the Advanced Research Projects Agency, U. S. Department of Defense under Contract DA-28-043-AMC-00394(E).

REFERENCES

(1) Arnal, R., "On the Initiation of Electric Discharges in Vacuum", C. R. Acad. Sci (Paris), 238, 2061 (1954); "Electric Microdischarges in Dynamic Vacuum", Ann. Phys. (Paris), 10, 830 (1955); Available as Translation USAEC-TR-2837.

(2) Mansfield, W. K., "Prebreakdown Conduction in Continuously Pumped Vacuum Systems", Brit. J. Appl. Phys., 11, 454 (1960).

(3) Pivovar, L. I. and Gordienko, V. I., "Microdischarges and Predischarges Between Metal Electrodes in High Vacuum", Soviet Physics,

Technical Physics, 28, 2101 (1958); "Prebreakdown Conduction Between Electrodes in Ultrahigh and High Vacuum", Soviet Physics - Technical Physics, 7, 908 (1963).

(4) Evans, R. D., "The Atomic Nucleus", Chapt. 20, 21, McGraw-Hill (1955).

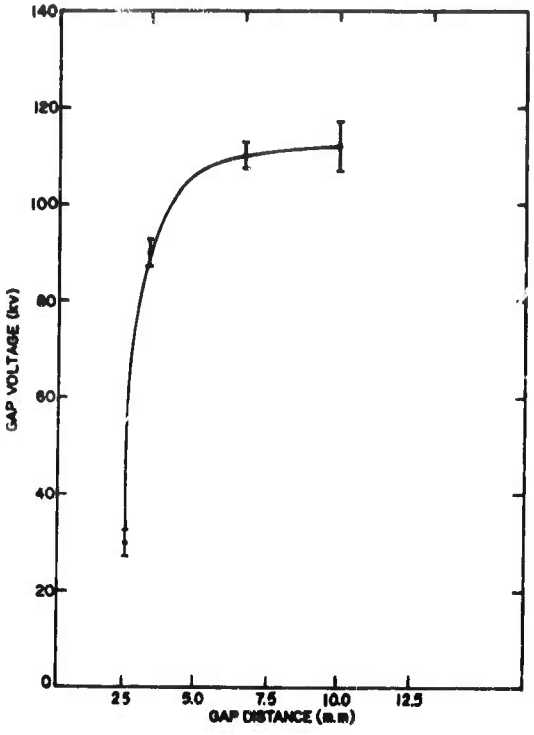

Figure 1. Variation of Microdischarge Threshold Voltage as a Function of Gap Distance

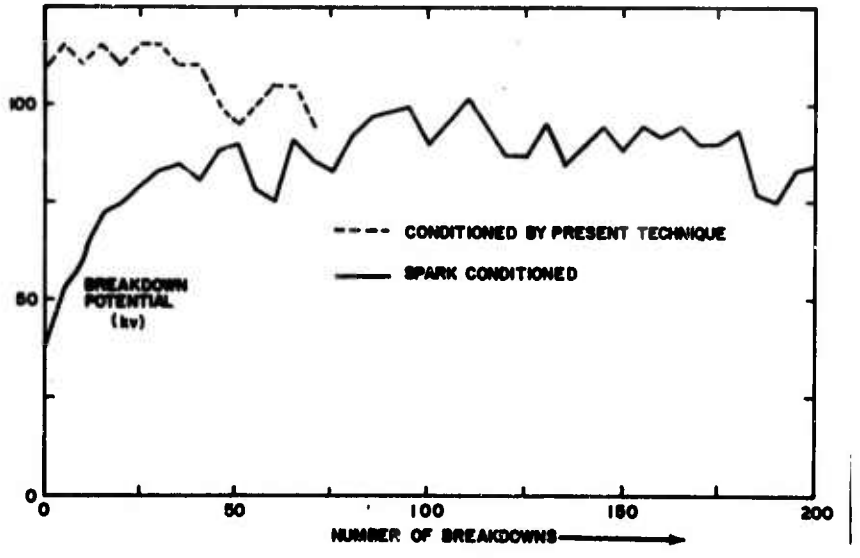

Figure 2. Comparison of Breakdown Sequence Diagrams for Electrodes Conditioned by Sparking and by Present Technique (Gap = 2.5 mm, Pressure = 5×10^{-7} Torr)

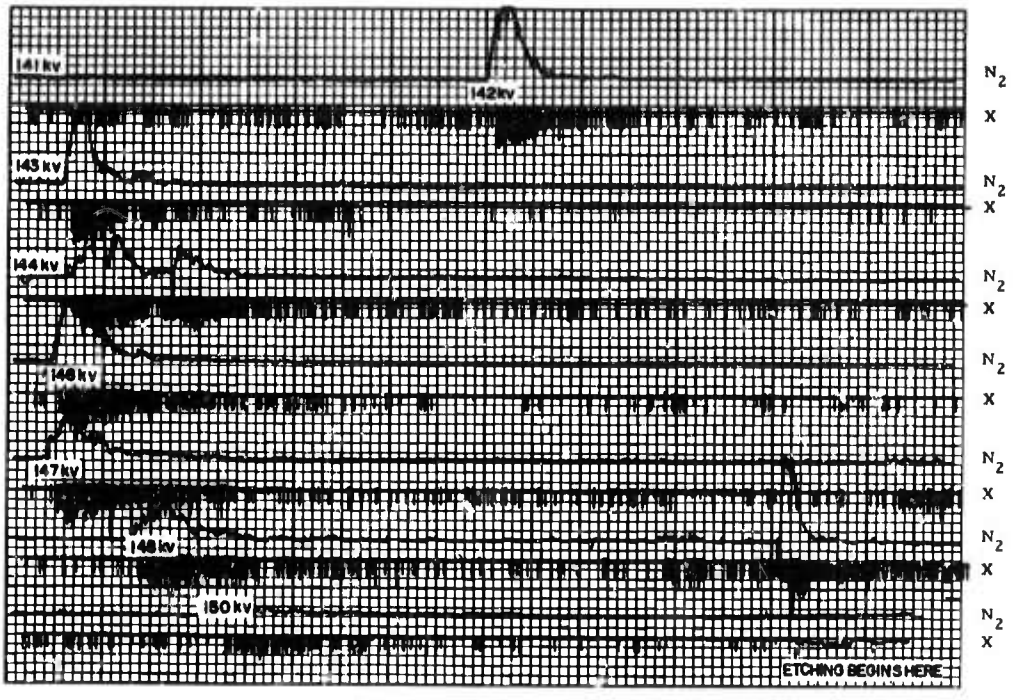

Figure 3. Simultaneous Recording of N_2 Partial Pressure and X-Ray Output

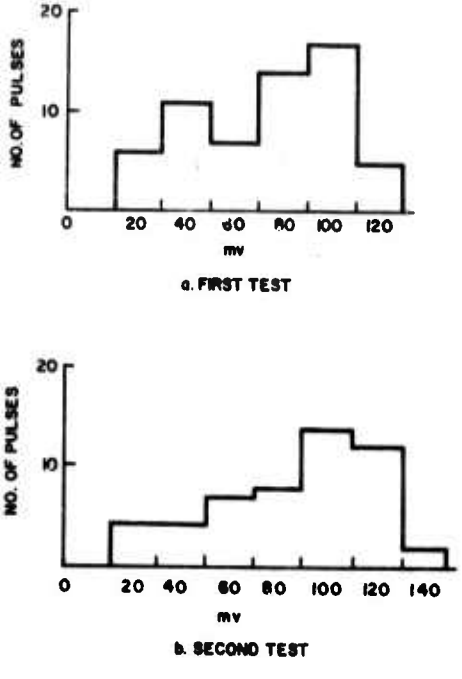

Figure 4. Experimentally Determined Pulse Height Spectra of X-Rays During Conditioning

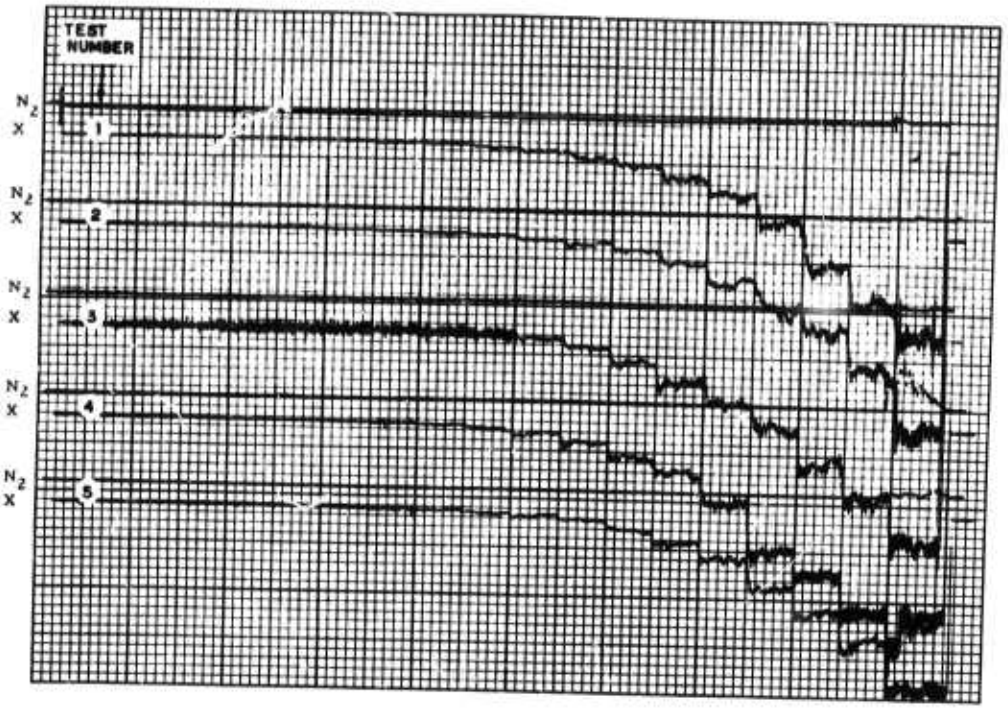

Figure 5. Typical Recording of X-Radiation from Etched Surface as the Voltage is Increased in Steps

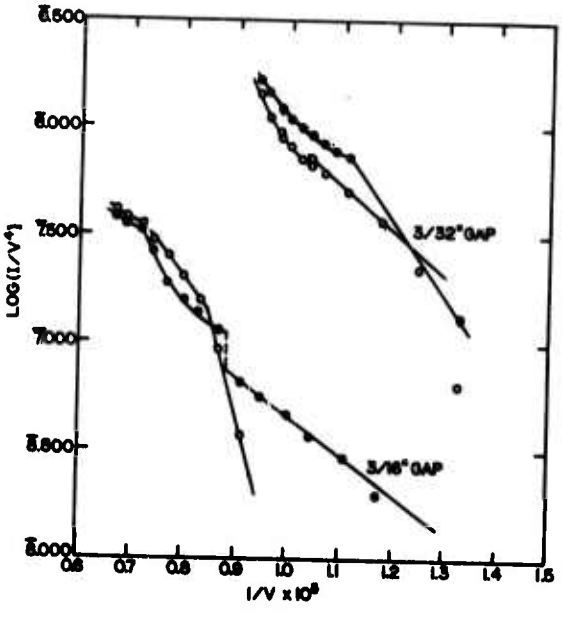

Figure 6. Equivalent Fowler-Nordheim Plots of X-Ray Output Showing Result of Variations in Field Enhancement Factor and Effective Emitting Surface Area

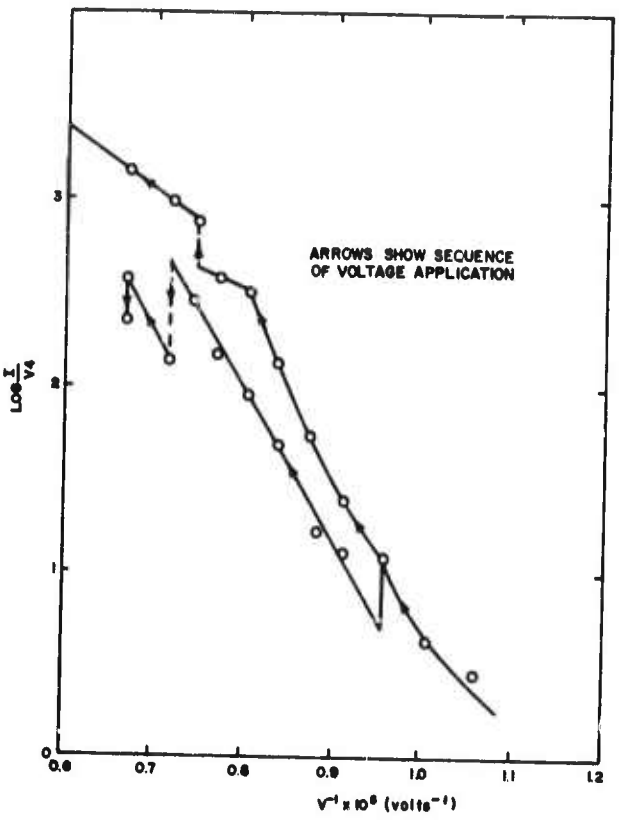

Figure 7. Fowler-Nordheim Plots for Two Consecutive Voltage Applications Without Breakdown

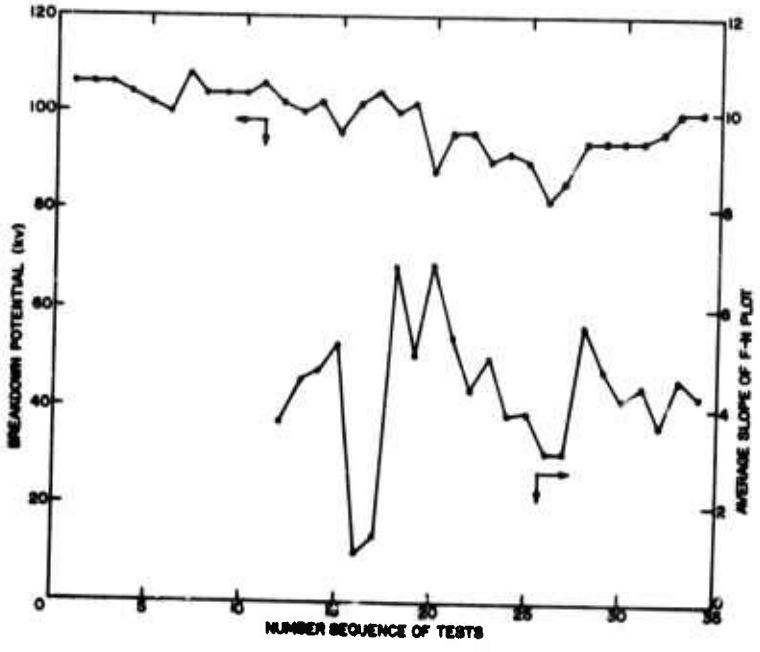

Figure 8. Sequence of Diagrams of Breakdown Voltages with the Corresponding Average Enhancement Factors

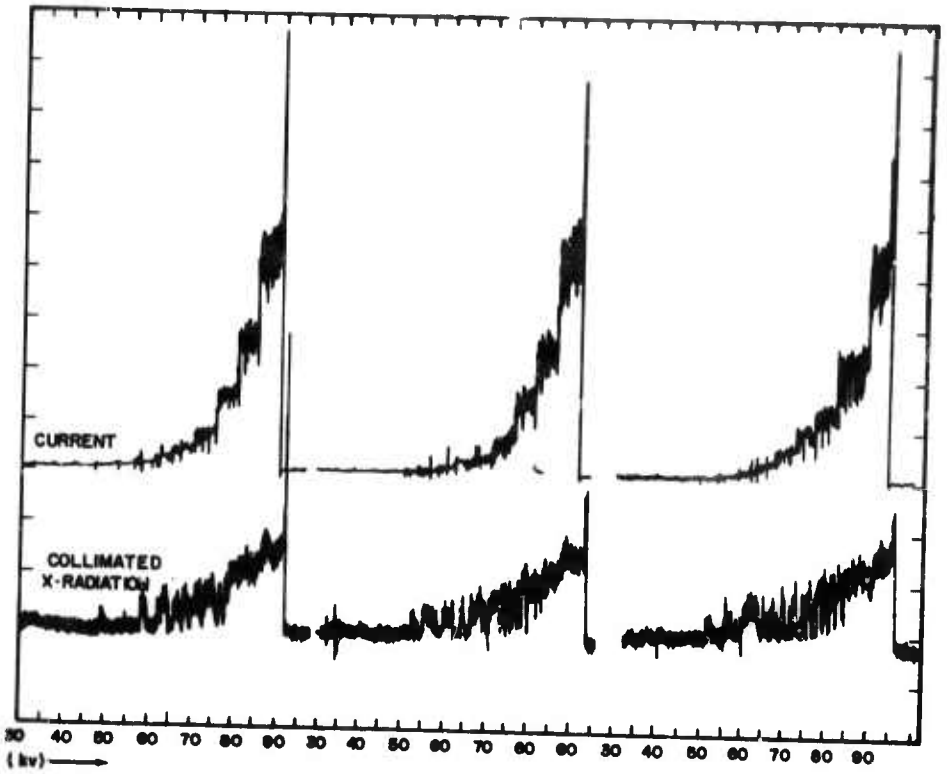

Figure 9. Current and Collimated X-Radiation as a Function of Voltage for Three Consecutive Step Tests

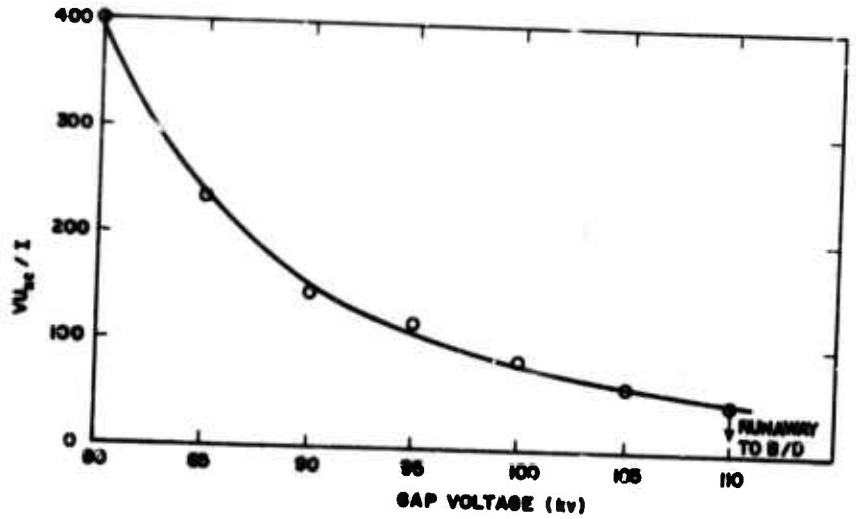

Figure 10. Variation of Effective Interelectrode Gas Density Calculated from Experimental Results

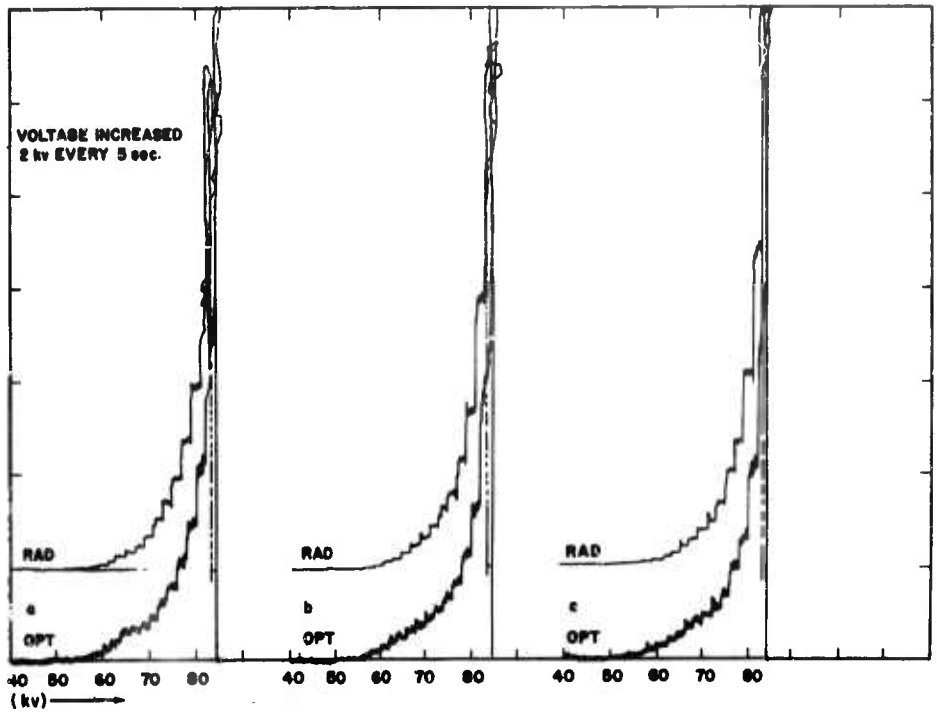

Figure 11. Typical Recordings of Visible and X-Radiation (2.5 mm Gap)

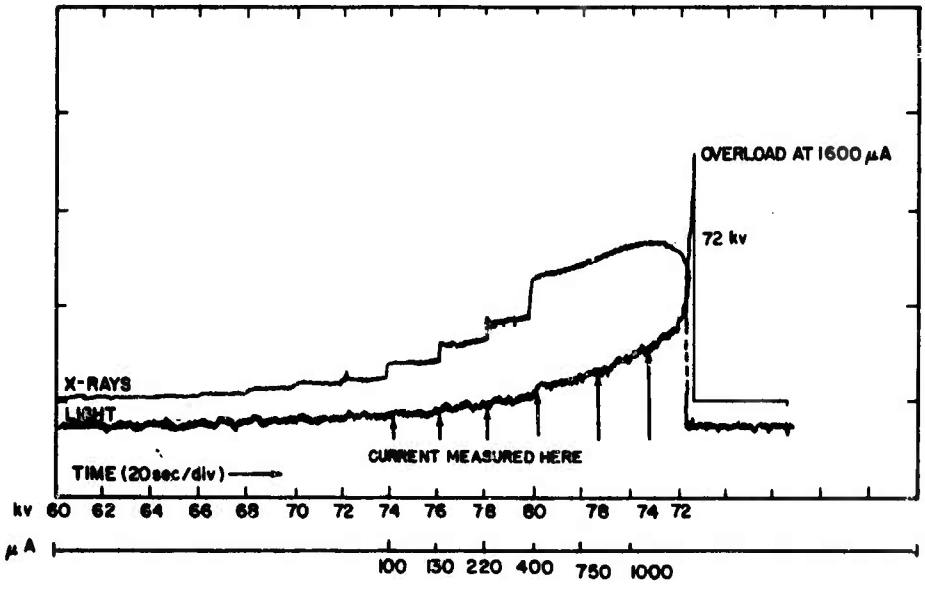

Figure 12. Visible and X-Ray Recording Demonstrating Runaway

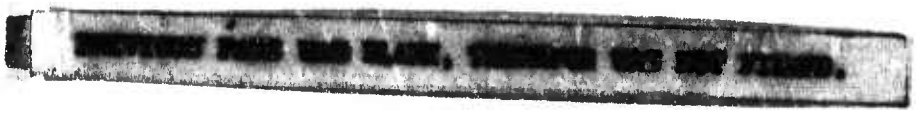

APPENDIX 5

DESIGNED EXPERIMENTS ON HIGH VOLTAGE VACUUM BREAKDOWN

DESIGNED EXPERIMENTS ON HIGH VOLTAGE VACUUM BREAKDOWN

by

M. J. Mulcahy, A. S. Denholm and A. Watson
Ion Physics Corporation

and

G. Taylor and M. Chrepta
U. S. Army Electronics Command

INTRODUCTION

An experiment has been designed to study the factors influencing high voltage vacuum breakdown under conditions pertinent to high power tube operation at 100 to 300 kv. The need for this has been generated by present-day requirements for extremely high power radar and communication systems, high energy particle accelerators and ion-propulsion systems. The demand is greatest in components such as vacuum tubes, vacuum capacitors and ion-propulsion systems where high voltage must be insulated by vacuum in small spaces. Therefore a reliable relation between the hold-off voltage and the factor or factors that affect electrical breakdown in vacuum is needed for the design of these components.

A second reason for this study is that, in spite of the voluminous literature on the subject, there are insufficient data available to permit a straightforward approach to the design of high-voltage sections of high-power electron tubes and other devices. Indeed a study of this literature shows a wide divergence in both the data and the theories that have been generated from the data. Figure 1 shows the spread of data from experiments by a number of investigators. These experiments were carried out in the traditional manner, varying the distance between electrodes and recording a breakdown voltage for that spacing. The experimental conditions such as preparation, material, finish and area of electrodes, pressure, contamination level and method of voltage application varied between one experiment and another. In some cases conditions which can be significant were not specified.

For these reasons, therefore, it was decided to carry out a statistically designed controlled experiment on the factors which affect voltage breakdown in vacuum in the range 100 to 300 kv. The statistical approach was chosen because it provides a powerful tool for the analysis of the results and enables information to be derived from a minimum number of experiments on the effects of the individual factors and as many of the joint effects of two or more factors as are required.

FACTORS AFFECTING BREAKDOWN

The 16 factors shown in Table 1 were considered the most likely contributors to the breakdown process. They are separated into two groups, flexible and inflexible. The flexible factors can all be varied continuously without disturbing the test setup. The inflexible factors, on the other hand, are constructional and with the exception of bakeout they cannot be varied without opening the vacuum test chamber. It was also recognized that the last four of the inflexible factors were concerned with a particular application and they were dropped from the initial investigation to reduce the complexity and accelerate the investigation. They will be introduced into the next phase of the experiment.

Meanwhile the remaining factors will be investigated at two levels. It is of interest to note here that the magnetic field may be regarded as three factors; namely, horizontal, vertical and oblique.

APPARATUS

The apparatus has to satisfy the following requirements. The vacuum test chamber should evacuate to 10^{-9} torr and be free of organic contamination. Further, it is required to bake to 400°C either the chamber and contents or the electrodes alone. Within the chamber a voltage up to 300 kv is specified for application across the electrode gap, and in some experiments a magnetic field of 500 gauss is required either perpendicular or parallel to the electric field vector. Finally, two energy storage levels, 100 J and 7000 kJ, are desired together with the facility for crowbarring in the latter case at variable times after initiation of a vacuum breakdown. The monitoring instrumentation developed during a preliminary experiment[1] is fitted to provide a continuous recording of the total and collimated X-radiation, the visible radiation, the gap current magnitude and wave shape and the partial pressure of hydrogen.

The test vehicle is shown in Figure 2. The vacuum chamber is made by welding together two spun hemispherical sections of 304 stainless steel, 36 inches diameter by 1-1/8 inch thick. This thickness eliminates the need for welded flanges at the ports. The chamber is equipped with three 16 inch diameter ports. One is at the top for the electrode support and adjusting mechanism, another at the bottom for the bakeable feedthrough bushing, and the third at the side for access and electrode changes. There is also a 10 inch port for the ion pump, and 6 inch ports are available for optical and X-ray detectors, a mass spectrometer, cryo pump and controlled leak valve. Gold or copper O-ring seals are used throughout.

The power supply is a Van de Graaff generator located in its pressure vessel beneath the vacuum chamber (Figure 2). It has a stabilizing circuit which reduces the ripple and long term fluctuations to less than 1% and it provides precise voltage control up to 300 kv with a maximum current of 200 μA. It is connected to the electrodes via a 100 ohm resistor and the

bakeable feedthrough bushing and has in parallel a 12 foot length of high voltage cable which both aids in the stabilization and stores about 20 joules of energy, or serves as connection with the larger energy store. The design of the feedthrough bushing is shown in Figure 3 and is described in detail elsewhere.[2] It consists of a bakeable ceramic-copper column which extends into the vacuum chamber and an unbakeable glass-aluminum column located in the Van de Graaff pressure tank. The ceramic column is brazed via a Monel alloy 404 flexure ring to a stainless steel flange and the latter makes a gold O-ring seal at the bottom port. The two columns are held together using a stainless steel tension rod which also carries the heater and thermocouple leads for the high voltage electrode. The bushing is pressurized to 45 psia SF_6 and voltage grading is effected using a solid dielectric insert with a spiral groove along which are wound two strings of 100 megohm resistors, one for each column. This insert also provides axial insulation at the ground plane.

Two electrode materials, OFHC copper and forged Ti-7Al-4Mo alloy have been used to date. The electrodes are 3 inches in diameter and either spherical or Bruce profile.[3] The anode is fixed in location on top of the bakeable feedthrough bushing while the insulating support and adjusting mechanism for the cathode consists of a welded bellows construction which enables gaps up to 3 cm to be obtained. The cathode support system was designed with a minimum of stray capacitance to permit fast current monitoring. Heaters and thermocouples are located in each electrode so that they could be baked independently of the system.

The requirement of producing a magnetic field of 500 gauss in any selected direction relative to the electrode geometry was achieved using water-cooled crossed coils (Figure 4) which could be dropped over the chamber for test and removed during system bakeout. The dimensions are as follows:

Coil	Mean Radius	Copper Weight	Approximate Power
Inner	56.00 cm	430 lb	12.5 kw
Outer	67.44 cm	610 lb	17.0 kw

The 7000 joule energy storage unit consists of four 80 kv, 0.6 μf cylindrical Tobe Deutschmann capacitors 20 inches high and 13 inches in diameter. They are stacked vertically as shown in Figure 5 with grading resistors housed axially inside each unit in a vessel pressurized to 2 atmospheres of SF_6. Figure 5 also shows the location of the grounding mechanism and the crowbar. The control and logic circuitry is so designed that it will cause the crowbar to fire and divert the stored energy at predetermined times after initiation of the main gap breakdown.

SEVEN FACTOR PILOT EXPERIMENT

In applying the statistical design to experiments on vacuum breakdown it was decided to conduct initially a two level, seven factor pilot experiment.

This experiment should show that all factors are under adequate control and provide information on the effect of varying the most likely factors and in particular on the importance of system bakeout. A one-fourth replicate factorial design involving 32 runs or treatments was chosen.[4] From this the importance of all factors can be determined but not all the interactions.

The factors for this pilot experiment were chosen on a basis of potential importance and the simplicity with which they could be varied. In fact they consisted of the first seven inflexible factors listed in Table 1.

The selection of a particular experimental design and the assigning of letters to the factors determines which two-factor interactions are confounded. First, therefore, the several processes which have been proposed for breakdown were considered including field emission dependent processes, the clump mechanism and microdischarge effects. The resultant assignment of letters to factors is shown in Table 2. The factors are represented by the letters A-G and the levels, high and low, by the letters a-g or the numeral 1, respectively. From this the main factor reactions and all but the following two factor interactions are measurable, AB, CE, AC, BE, AE, and BC, and also the effect of any two factor interaction involving the bakeout factor D is clear of any other main effect or two-factor interaction of interest.

The order of the 32 experiments was determined in a random manner and then arranged in a circle as shown in Figure 6. It is statistically acceptable to initiate the pilot experiment at any point of the circle and then to proceed either clockwise or counterclockwise. Treatment "bdefg" was chosen as the starting point and it was decided to proceed in the clockwise direction. The factor level for all treatments is shown in Table 3. Thus, for this first experiment the electrodes only were baked and they were both highly polished titanium and of Bruce profile. Just prior to this the complete system was baked out, ensuring a clean test vehicle at the outset of the experiment.

PROCEDURES

Controlled procedures are, of course, essential to reproducible results and good control is mandatory for the designed experiment. Methods for electrode preparation, installation, bakeout and voltage application were determined, and used to standardize the levels of the factors to be examined and to keep constant those factors to be held invariant.

Electrode Preparation and Installation

For coarse finish the electrode surfaces are wet ground with silicon carbide paper using successively finer grits in the sequence 180, 320, 400 and 600. For fine finish the surfaces after grinding are polished with 15 micron alumina abrasive, and then with microcloth and alumina abrasives of 5, 1, 0.3 and 0.05 micron size both using a powered felt covered wheel or a spindle and by hand. At the termination of the grinding or polishing operations the electrodes were rinsed in water and methyl alcohol and dried in hot

air. Just prior to assembly in the test chamber they are rinsed in acetone and trichloroethylene and wiped with acetone and methanol using cheese cloths. Finally, they are wiped with Foamwipes in the chamber. During electrode installation the chamber is continuously flushed with dry nitrogen which exits through the access port.

Bakeout

The baking cycle for both system and electrode bakeout was fixed at 16 hours. This breaks down as 12 hours for the electrodes between 400°C and 450°C, and 8 hours for the chamber between 350°C and 400°C. In each case, the electrodes are allowed to cool to less than 75°C before test initiation. The pressure then is low 10^{-7} torr to mid 10^{-8} torr region for electrode only bakeout and low 10^{-8} torr region for system bakeout.

Voltage Application

The gap is initially set at 1.0 cm and the voltage increased in 10 kv increments every two minutes up to breakdown. The voltage is not switched off and is further increased at the same rate to a second breakdown after which the supply is switched off. This gives points 1 and 2 on Figure 7. The voltage is then increased rapidly to within 10 kv of the first breakdown voltage and then in 10 kv steps every two minutes until breakdown (point 3 of Figure 7). The gap is then set successively at 1.5, 2.0, 2.5, 3.0 and 0.5 cm, and the voltage increased rapidly to within 10 kv of the previous breakdown and then in 10 kv increments to breakdown, except in the 0.5 cm case when it is increased rapidly to 60 kv. This gives points 4, 5, 6, 7 and 8 of Figure 7. The gap is then re-set to 1.0 cm, the breakdown voltage checked (point 9) and the gap conditioned by sparking until the voltage is increased by about 30%. The voltage is then switched off and conditioned breakdown voltages obtained for all gaps (points 10 through 16).

During these operations the following parameters are continuously recorded: total and collimated X-radiation, optical radiation, H_2 partial pressure and gap current. The current wave shapes are also monitored on an oscilloscope.

RESULTS

At the time of writing, 28 of the 32 treatments in the pilot experiment have been completed. Of these, 14 involved system bakeout and 14 electrode only bakeout. It is of interest to note here that, including the bakeouts during system checkout, the ceramic-copper column (22 brazed ceramic/metal seals) has now undergone 18 bakeouts in the range 300 to 400°C and operates satisfactorily to 300 kv.

Statistical Analysis

The unconditioned and conditioned breakdown values for the 1.0 cm gap have been used for the analysis which was carried out in treatments 5 through 28; i.e., 24 treatments. However, before presenting the results of this

analysis and discussing the trends, the objectives of the pilot experiment should be borne in mind. Apart from investigation of the effects of the seven factors, these were familiarization with the apparatus and with the statistical technique and finalization of a procedure which could be used for all future tests. In fact, the procedure described in this paper was not finalized until after about 9 treatments had been completed. Within this frame of reference, the analysis to date has yielded the following:

1. The trends for the unconditioned values are given in Table 4. Positive signs signify that the breakdown voltage is increased when the relevant factor or factors are at the higher level and decreased when they are at the lower level; negative signs signify the reverse. Thus, for example, examining shape factor B, when the cathode geometry is Bruce profile the voltage is reduced by 6. 7 kv and increased by 6. 7 kv when the cathode is a sphere. However, since the standard deviation is 6. 7, there is a low level of confidence in the trends of Table 4, especially beyond the top four. An encouraging factor, however, is that this standard deviation has decreased from 7. 4 for 22 treatments to the present value of 6. 7 for 24 treatments.

2. The trends for the conditioned breakdowns exhibit a wider scatter such that the level of confidence is zero, a not surprising result considering the almost inherent uncertainties of the conditioning process; for example, after conditioning material transfer has occurred. In some cases strong etches appeared which persisted, while in other cases no etches appeared or they quickly disappeared. This is being examined further with a view to standardizing this process.

3. There is a trend towards increasing breakdown voltage with run number, as though the apparatus and/or the electrodes are undergoing long-term conditioning. The slope of this trend curve for electrode only bakeout is three times that for system bakeout.

4. There is indication that the history of the electrodes may have some significance. However, no conclusions are warranted as yet.

Physical Analysis

It has been found that for gaps up to 1. 5 cm the breakdown voltage varies approximately as the square root of the gap separation for both conditioned and unconditioned electrodes. The results were therefore plotted as a function of the square root of the gap separation (Bruce-Bruce configuration) or equivalent gap separation (Bruce-sphere configuration). Equivalent gap separation is the uniform field spacing to give the same cathode field strength. A plot of voltage against the square root of this equivalent spacing should give a straight line from both the uniform and non-uniform field criteria proposed by Cranberg.(5) Typical plots are shown in Figures 7 and 8. From these it can be seen that for gaps greater than 1. 5 cm, not only does the voltage deviate from the half-power relationship but that it sometimes decreases before again increasing. This is a consistent effect but, the gap length at which it takes place varies.

Both voltage and current relationships are being analyzed at present and will be reported at a later date.

CONCLUSIONS

The main statistical conclusion to date is that the effect of no factor of simple combination of factors has proved strong enough to overcome the standard deviation or error function. This may be explained partly by the fact that the experiment is not yet complete and also by the fact that the procedure was not finalized until about 9 treatments had been completed. However, the possibility should not be ruled out that variations in the level of some uncontrolled factor may be responsible. Such a factor, for example, may be the bakeout temperature or the gas content of the electrodes. More meaningful conclusions will be drawn when the pilot experiment has been completed and the earlier treatments repeated.

Meanwhile, even these preliminary treatments have been of great value in that they have highlighted the need for controlled experimentation in vacuum breakdown to get meaningful results, and also the danger of drawing unwarranted conclusions from insufficient data. Several parts of this experiment, if conducted in isolation, could easily have led to conclusions which are shown to be unwarranted by the total experiment to date.

Theories as to the physics of the vacuum breakdown mechanism in the range 100 to 300 kv, and how this is affected by the various factors, will be withheld until the experiment and current analysis has been completed.

ACKNOWLEDGMENTS

The authors acknowledge with pleasure the assistance of G. K. Simcox, M. M. Thayer and F. J. McCoy in designing the apparatus; that of R. Parsons and C. Boudreau in maintaining it and taking results; and R. Bristow of General Electric Company who was responsible in part for the design of the bakeable ceramic/metal column and wholly responsible for its fabrication. Finally, the help of J. Weinstein in drawing up the statistical design and carrying out the analysis is acknowledged.

This work was sponsored by the Advanced Research Projects Agency, U. S. Department of Defense under Contract DA-28-043-AMC-00394(E).

REFERENCES

1. Watson, A., Denholm, A. S. and Mulcahy, M. J., "Prebreakdown Phenomena in Vacuum Gaps", Second International Symposium on High Voltage Insulation in Vacuum (1966).

2. "High Voltage Breakdown Study", Quarterly Progress Reports 1 through 5, Contract DA-28-043-AMC-00394(E), Ion Physics Corporation, Burlington, Massachusetts (16 November 1964 through 15 February 1966).

3. Bruce, F. M., "Calibration of Uniform Field Spark Gaps for High Voltage Measurement at Power Frequencies", Proc. IEEE, 94, Pt. 2, 138 (1947).

4. Chrepta, M. M., Weinstein, J., Taylor, G. W. and Zinn, M. H., "The Design of a High-Voltage Breakdown-in-Vacuum Experiment", Conference on Design of Experiments, sponsored by Army Research Office (1965).

5. Cranberg, L., "The Initiation of Electrical Breakdown in Vacuum", J. Appl. Phys., 26, 596 (1955).

Table 1. Inflexible and Flexible Factors

Inflexible Factors	Flexible Factors
1. Cathode Material	12. Residual Gas Pressure
2. Anode Material	13. Energy of Supply
3. Cathode Finish	14. Contaminant
4. Anode Finish	15. Magnetic Field
5. Cathode Geometry	16. Electrode Spacing
6. Anode Geometry	
7. Vehicle Bakeout	
8. Envelope Material	
9. Envelope Diameter	
10. Electrode Shield Size	
11. Electrode Shield Placement	

Table 2. Factors and Levels for Pilot Experiment

Factors	Letters	Levels
Cathode Material	C	1 - Ti-7Al-4Mo c - OFHC Cu
Cathode Finish	G	g - Fine 1 - Coarse
Cathode Geometry	B	b - Bruce Profile 1 - Sphere
Bakeout	D	1 - Complete System Bakeout d - Electrode Bakeout Only
Anode Material	A	1 - Ti-7Al-4Mo a - OFHC Cu
Anode Finish	F	f - Fine 1 - Coarse
Anode Geometry	E	e - Bruce Profile 1 - Sphere

Table 3. Order and Factor Level for Pilot Experiment

Experiment	Material	Cathode Finish	Geometry	Bakeout	Material	Anode Finish	Geometry
bdefg	Ti	Fine	Bruce	Electrode	Ti	Fine	Bruce
abdf	Ti	Coarse	Bruce	Electrode	Cu	Fine	Sphere
fg	Ti	Fine	Sphere	System	Ti	Fine	Sphere
adefg	Ti	Fine	Sphere	Electrode	Cu	Fine	Bruce
bcd	Cu	Coarse	Bruce	Electrode	Ti	Coarse	Sphere
ade	Ti	Coarse	Sphere	Electrode	Cu	Coarse	Bruce
ab	Ti	Coarse	Bruce	System	Cu	Coarse	Sphere
beg	Ti	Fine	Bruce	System	Ti	Coarse	Bruce
bef	Ti	Coarse	Bruce	System	Ti	Fine	Bruce
acf	Cu	Coarse	Sphere	System	Cu	Fine	Sphere
abcdeg	Cu	Fine	Bruce	Electrode	Cu	Coarse	Bruce
ce	Cu	Coarse	Sphere	System	Ti	Coarse	Bruce
abfg	Ti	Fine	Bruce	System	Cu	Fine	Sphere
bcf	Cu	Coarse	Bruce	System	Ti	Fine	Sphere
abdg	Ti	Fine	Bruce	Electrode	Cu	Coarse	Sphere
cdeg	Cu	Fine	Sphere	Electrode	Ti	Coarse	Bruce
bde	Ti	Coarse	Bruce	Electrode	Ti	Coarse	Bruce
dg	Ti	Fine	Sphere	Electrode	Ti	Coarse	Sphere
acd	Cu	Coarse	Sphere	Electrode	Cu	Coarse	Sphere
abce	Cu	Coarse	Bruce	System	Cu	Coarse	Bruce
aeg	Ti	Fine	Sphere	System	Cu	Coarse	Bruce
abcefg	Cu	Fine	Bruce	System	Cu	Fine	Bruce
bcdfg	Cu	Fine	Bruce	Electrode	Ti	Fine	Sphere
acg	Cu	Fine	Sphere	System	Cu	Coarse	Sphere
aef	Ti	Coarse	Sphere	System	Cu	Fine	Bruce
(1)	Ti	Coarse	Sphere	System	Ti	Coarse	Sphere
cdef	Cu	Coarse	Sphere	Electrode	Ti	Fine	Bruce
acdfg	Cu	Fine	Sphere	Electrode	Cu	Fine	Sphere
abcdef	Cu	Coarse	Bruce	Electrode	Cu	Fine	Bruce
cefg	Cu	Fine	Sphere	System	Ti	Fine	Bruce
df	Ti	Coarse	Sphere	Electrode	Ti	Fine	Sphere
bcg	Cu	Fine	Bruce	System	Ti	Coarse	Sphere

Table 4. Trends for Unconditioned Breakdown Voltages of 1.0 cm Gaps (Treatments 5 through 28)

Factors	Trend
AE + BC	-9.0
D	+7.0
B	-6.7
BD	-6.5
E	-6.2
AB + CE	-5.3
AG	-4.4
AD	+4.1
CD	+3.8
DG	-3.7
C	+3.5
G	+3.4
EG	-3.4
BE + AC	+3.4
DE	+2.7
A	-2.5
EF	-2.2
F	+2.1
AF	-2.1
CF	+2.0
DF	+1.8
BG	-1.8
FG	+1.3
BF	-0.8
CG	-0.2

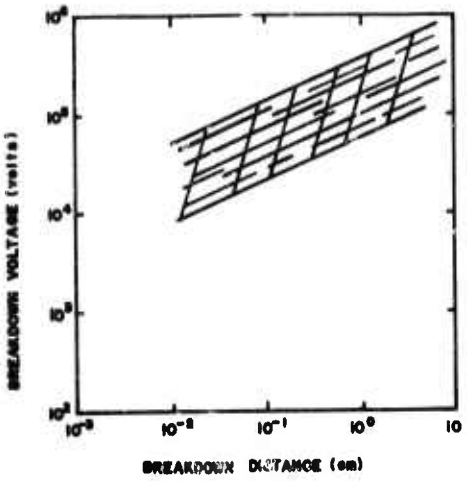

Figure 1. Spread in Vacuum Breakdown Voltage Reported in the Literature

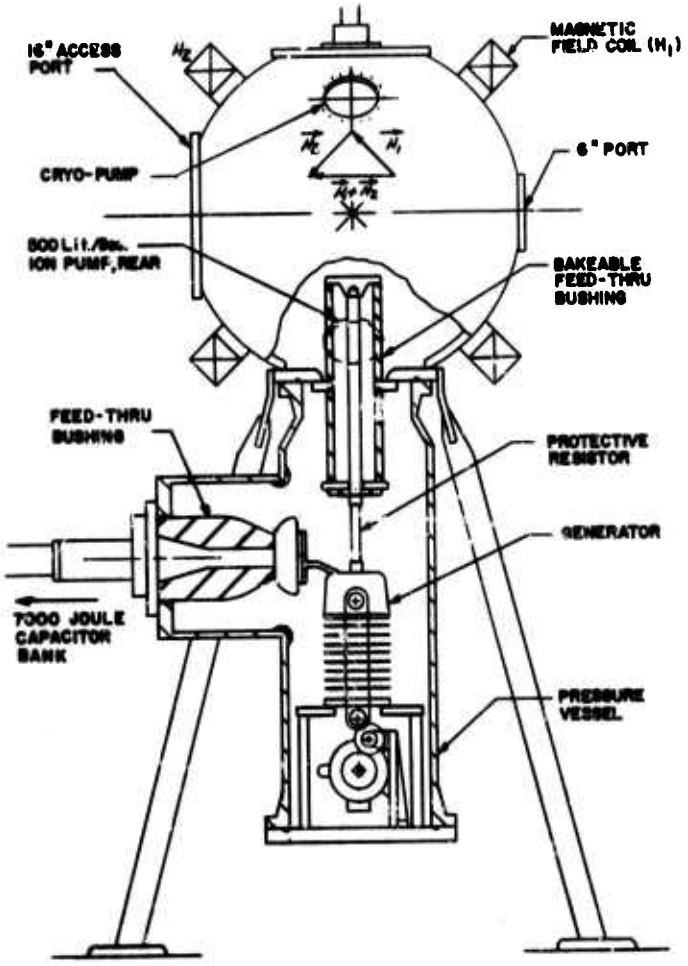

Figure 2. 300 kv Test Vehicle

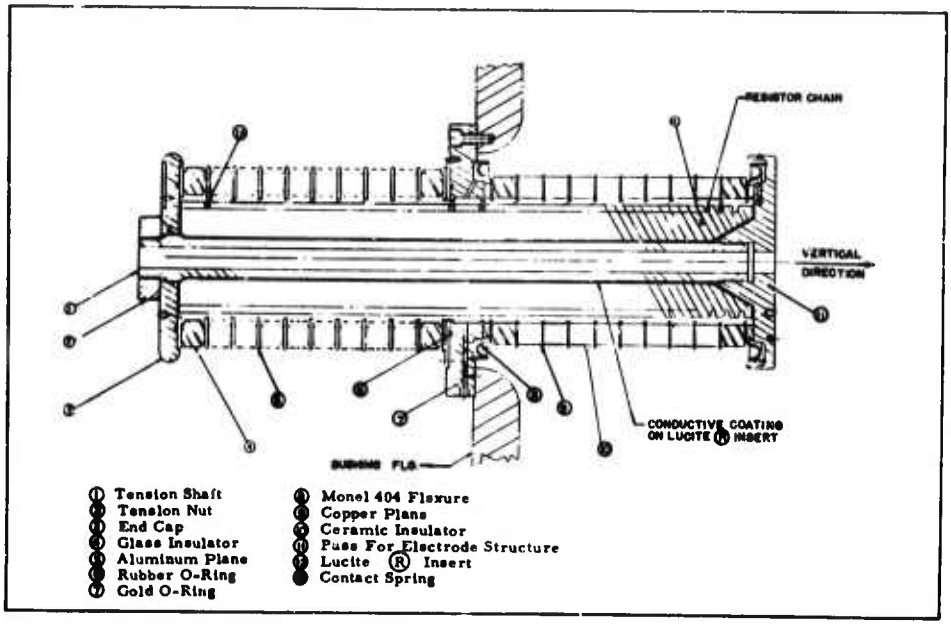

Figure 3. Bakeable Feedthrough Bushing

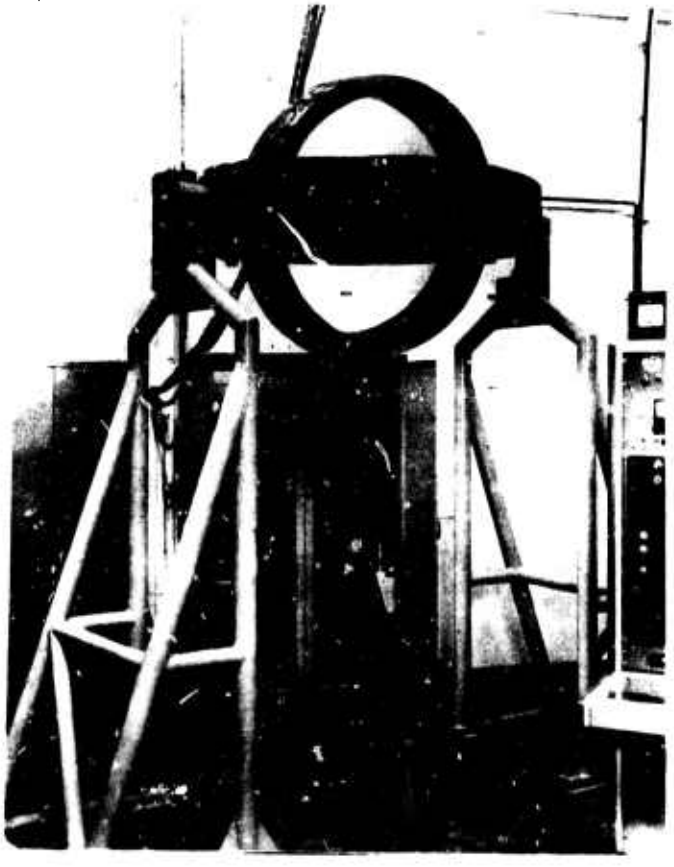

Figure 4. 500 Gauss Magnetic Field Coils and Power Supply

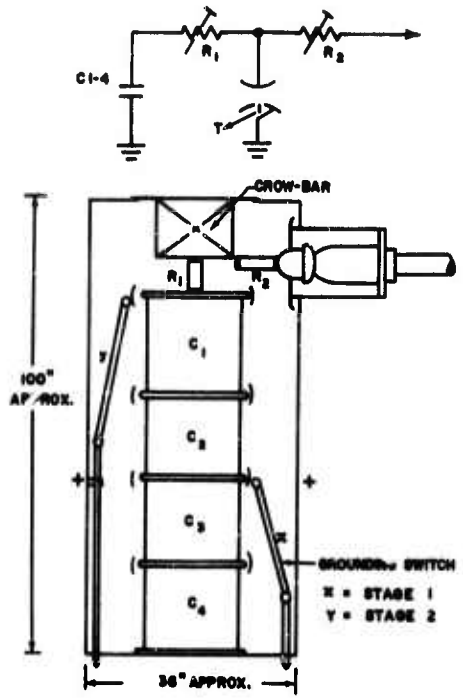

Figure 5. Outline of 300 kv Energy Storage System with Crowbar

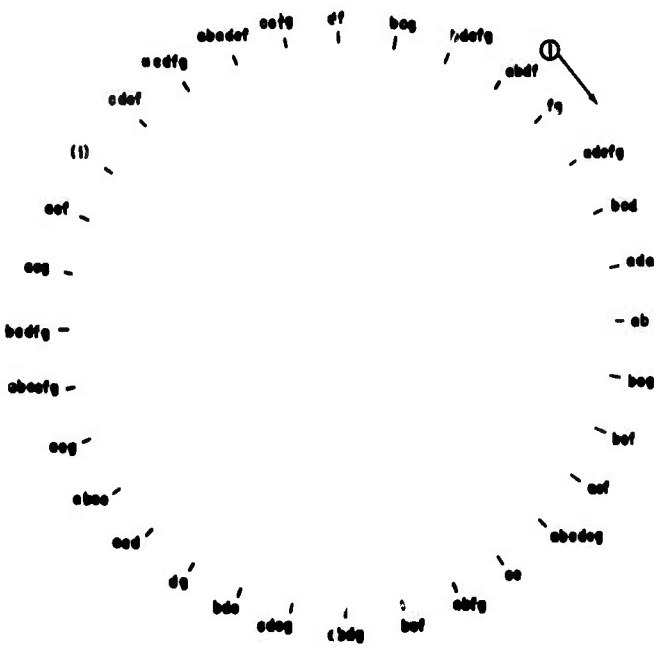

Figure 6. Random Selection Wheel for Pilot Experiment

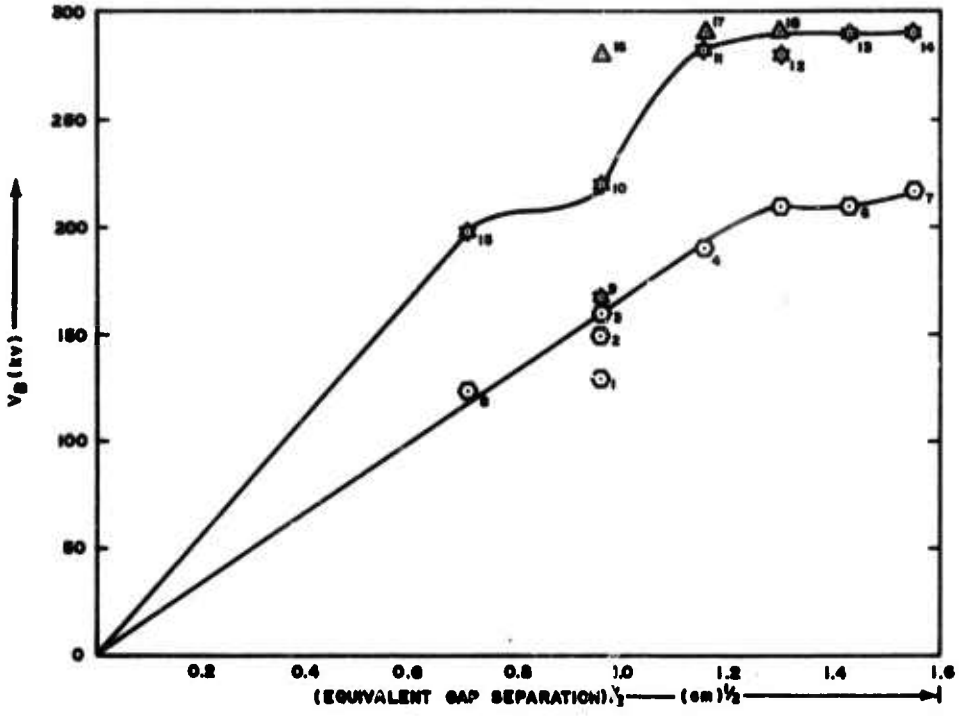

Figure 7. Sequence of Breakdowns for Treatment 'acg'

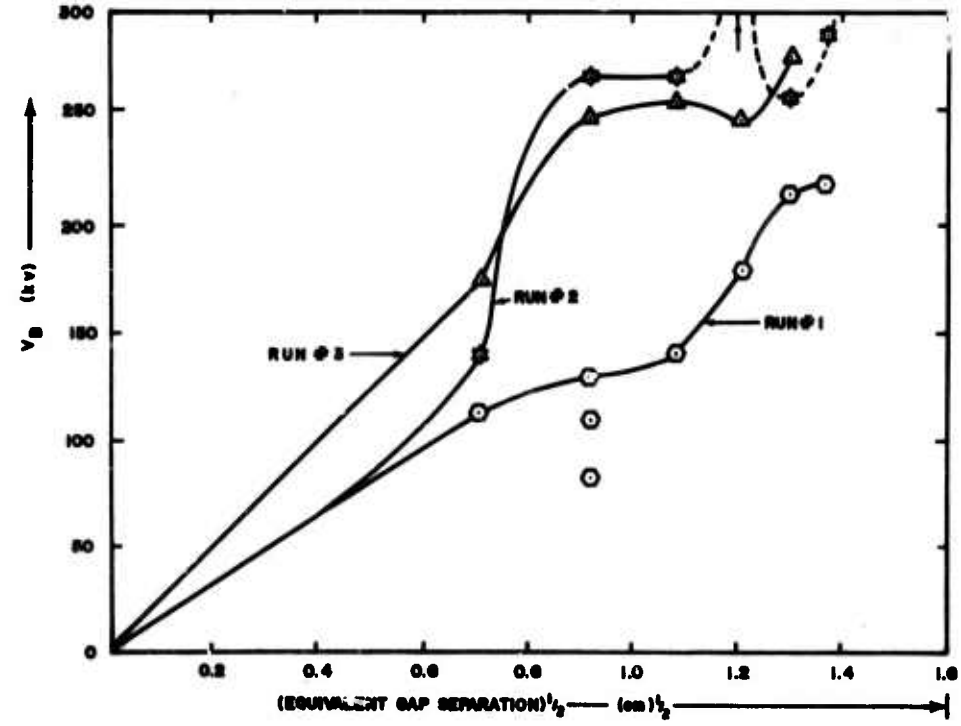

Figure 8. Unconditioned and Conditioned Breakdown Voltages for Treatment '(1)'

APPENDIX 6

VACUUM BREAKDOWN AS A FUNCTION OF GAP SEPARATION

VACUUM BREAKDOWN AS A FUNCTION OF GAP SEPARATION*

A. Watson and M. J. Mulcahy
Ion Physics Corporation

Vacuum breakdown voltages up to 300 kv were measured at gap separations from 0.5 to 3.0 cm. Two experimental techniques were compared. First, the voltage was raised in steps for each gap separation, recording the first isolated breakdown and terminating the test. Second, the voltage was increased, neglecting isolated sparks, until repetitive sparking occurred. Both techniques yielded curves of the breakdown voltage as a function of gap separation at various stages of conditioning by sparking. Other curves were similarly obtained after leaving the vacuum system to decondition. The repetitive sparking voltage, but not the isolated sparking voltage, varied approximately linearly with the square root of the gap separation. The logarithm of the current immediately prior to breakdown was plotted as a function of the square root of gap separation for both techniques. A linear decrease was observed for repetitive sparking but no such trend appeared with isolated breakdown until after deconditioning. When the electrodes only were baked at 400°C, as opposed to the complete system, pressure surges of hydrogen were observed just below the breakdown voltage.

---

* Work sponsored by the Advanced Research Projects Agency, U.S. Department of Defense.

Security Classification

DOCUMENT CONTROL DATA - R&D

(Security classification of title, body of abstract and indexing annotation must be entered when the overall report is classified)

1. ORIGINATING ACTIVITY *(Corporate author)* Ion Physics Corporation Burlington, Massachusetts	2a. REPORT SECURITY CLASSIFICATION UNCLASSIFIED 2b. GROUP N/A

3. REPORT TITLE

HIGH VOLTAGE BREAKDOWN STUDY

4. DESCRIPTIVE NOTES *(Type of report and inclusive dates)*

Eighth Quarterly Progress Report, 16 August 1966 through 15 November 1966

5. AUTHOR(S) *(Last name, first name, initial)*

M. J. Mulcahy and A. Watson

6. REPORT DATE April 1967	7a. TOTAL NO. OF PAGES 103	7b. NO. OF REFS 15
8a. CONTRACT OR GRANT NO. DA-28-043-AMC-00394(E) b. PROJECT NO. 7900.21.243.40.00 c. TASK d.	9a. ORIGINATOR'S REPORT NUMBER(S) 9b. OTHER REPORT NO(S) *(Any other numbers that may be assigned this report)* ECOM-00394-F8	

10. AVAILABILITY/LIMITATION NOTICES

This document is subject to special export controls and each transmittal to foreign governments or foreign nationals may be made only with prior approval of CG, U.S. Army Electronics Command, Attn: AMSEL-KL-TS, Fort Monmouth, N. J.

11. SUPPLEMENTARY NOTES	12. SPONSORING MILITARY ACTIVITY U.S. Army Electronics Command Fort Monmouth, New Jersey 07703 AMSEL-KL-TS

13. ABSTRACT

The polot experiment has been completed involving 32 treatments and 16 replications; of these, 23 involved full system bakeout. Procedures are used which yielded the significant unconditioned and conditioned data for electrode gaps ranging from 1.5 to 3.0 cm. The results have been satistically analyzed and a unified theory of breakdown has been developed which is consistent with the trends of this analysis. Finally, the 300 kv system has been maintained in a fully operational state and assembly of the magnetic field and energy storage systems has continued.

DD FORM 1 JAN 64 1473

Security Classification

Security Classification

14. KEY WORDS	LINK A		LINK B		LINK C	
	ROLE	WT	ROLE	WT	ROLE	WT
Electrical Breakdown in Vacuum Conditioning Procedures Optical and X-Radiation Partial Pressure and Gap Current Etching Controlled Statistical Experiment						

INSTRUCTIONS

1. ORIGINATING ACTIVITY: Enter the name and address of the contractor, subcontractor, grantee, Department of Defense activity or other organization *(corporate author)* issuing the report.

2*a*. REPORT SECURITY CLASSIFICATION: Enter the overall security classification of the report. Indicate whether "Restricted Data" is included. Marking is to be in accordance with appropriate security regulations.

2*b*. GROUP: Automatic downgrading is specified in DoD Directive 5200.10 and Armed Forces Industrial Manual. Enter the group number. Also, when applicable, show that optional markings have been used for Group 3 and Group 4 as authorized.

3. REPORT TITLE: Enter the complete report title in all capital letters. Titles in all cases should be unclassified. If a meaningful title cannot be selected without classification, show title classification in all capitals in parenthesis immediately following the title.

4. DESCRIPTIVE NOTES: If appropriate, enter the type of report, e.g., interim, progress, summary, annual, or final. Give the inclusive dates when a specific reporting period is covered.

5. AUTHOR(S): Enter the name(s) of author(s) as shown on or in the report. Enter last name, first name, middle initial. If military, show rank and branch of service. The name of the principal author is an absolute minimum requirement.

6. REPORT DATE: Enter the date of the report as day, month, year, or month, year. If more than one date appears on the report, use date of publication.

7*a*. TOTAL NUMBER OF PAGES: The total page count should follow normal pagination procedures, i.e., enter the number of pages containing information.

7*b*. NUMBER OF REFERENCES: Enter the total number of references cited in the report.

8*a*. CONTRACT OR GRANT NUMBER: If appropriate, enter the applicable number of the contract or grant under which the report was written.

8*b*, 8*c*, & 8*d*. PROJECT NUMBER: Enter the appropriate military department identification, such as project number, subproject number, system numbers, task number, etc.

9*a*. ORIGINATOR'S REPORT NUMBER(S): Enter the official report number by which the document will be identified and controlled by the originating activity. This number must be unique to this report.

9*b*. OTHER REPORT NUMBER(S): If the report has been assigned any other report numbers *(either by the originator or by the sponsor)*, also enter this number(s).

10. AVAILABILITY/LIMITATION NOTICES: Enter any limitations on further dissemination of the report, other than those imposed by security classification, using standard statements such as:

(1) "Qualified requesters may obtain copies of this report from DDC."

(2) "Foreign announcement and dissemination of this report by DDC is not authorized."

(3) "U. S. Government agencies may obtain copies of this report directly from DDC. Other qualified DDC users shall request through

_____."

(4) "U. S. military agencies may obtain copies of this report directly from DDC. Other qualified users shall request through

_____."

(5) "All distribution of this report is controlled. Qualified DDC users shall request through

_____."

If the report has been furnished to the Office of Technical Services, Department of Commerce, for sale to the public, indicate this fact and enter the price, if known.

11. SUPPLEMENTARY NOTES: Use for additional explanatory notes.

12. SPONSORING MILITARY ACTIVITY: Enter the name of the departmental project office or laboratory sponsoring *(paying for)* the research and development. Include address.

13. ABSTRACT: Enter an abstract giving a brief and factual summary of the document indicative of the report, even though it may also appear elsewhere in the body of the technical report. If additional space is required, a continuation sheet shall be attached.

It is highly desirable that the abstract of classified reports be unclassified. Each paragraph of the abstract shall end with an indication of the military security classification of the information in the paragraph, represented as *(TS)*, *(S)*, *(C)*, or *(U)*.

There is no limitation on the length of the abstract. However, the suggested length is from 150 to 225 words.

14. KEY WORDS: Key words are technically meaningful terms or short phrases that characterize a report and may be used as index entries for cataloging the report. Key words must be selected so that no security classification is required. Identifiers, such as equipment model designation, trade name, military project code name, geographic location, may be used as key words but will be followed by an indication of technical context. The assignment of links, rules, and weights is optional.